Influence of Strain Rate and Temperature Upon the Mechanical and Fracture Behavior of a Simulated Solid Propellant

By

Hervé Mouille

Thesis submitted to the faculty of the

Virginia Polytechnic Institute and State University

in partial fulfillment of the requirements for the degree of

Master of Science

in

Engineering Science and Mechanics

APPROVED:

C.W. Smith, Chairman

D. Post

R.W. Landgraf

April, 1992

Blacksburg, Virginia

Influence of Strain Rate and Temperature Upon the Mechanical and Fracture Behavior of a Simulated Solid Propellant

By

Hervé Mouille

C. W. Smith, Chairman

Engineering Science and Mechanics

(Abstract)

The mechanical response of a simulated composite solid propellant is studied at temperatures of -65°F, 72°F and 165°F, and at test head rates of 2.54 and 12.7 mm/min. After determining the biaxial tensile stress-strain and stress relaxation responses of the material, crack propagation tests were conducted on single-edge, cracked biaxial specimens. The grid method was employed to obtain the local in-plane displacements and strains at the free surface near the crack tip. Moreover, a continuum algorithm based on the in-plane displacements was used to estimate the dominant displacement eigenvalue where the crack front intersected the free surface.

Over the range -65°F to 72°F, the effect of temperature upon the global mechanical response of the material is significant. By way of contrast, the effects of temperature and head rate over the ranges 72°F to 165°F and 2.54 to 12.7 mm/min., respectively, are quite small. Moreover, the crack propagation process is observed to be qualitatively temperature and head rate independent over the ranges investigated. Finally, the measurement of the dominant displacement eigenvalue at the free surface using a continuum algorithm has met some success.

Acknowledgements

The author wishes to express his sincere appreciation to his committee chairman, prof. C.W. Smith, for his assistance, guidance and friendship throughout the course of this research. Sincere appreciation is also extended to the other members of the author's advisory committee, Dr. D. Post and Dr. R.W. Landgraf, for their valuable advice and suggestions on the research and the thesis.

The support of Phillips Laboratory AFMC, under contract no. FO-4611-88-K-0025, and the guidance of Dr. C.T. Liu are acknowledged.

The author is also grateful to his friend and lad partner, Alex L. Wang, for his help and encouragement. The cooperation and friendship of the other author's labmates is also gratefully acknowledged.

The constant concern and friendship of Doris Smith and Frieda Post are appreciated.

The author is also thankful to his friends who made his three years at Virginia Tech a great and unique experience. Among them, Dr. R.G. Saacke, Ann Saacke, the brothers of the Zeta Beta chapter of Alpha Phi Omega, Peter Ifju, Marc Tricard, Christophe Vailhe, Scott Courtney and Theresa Gillespie.

Special thanks go to Région Rhone-Alpes, France and Fondation Arts et Métiers, Paris-France for granting the author.

Finally, the author wishes to thank his parents and family, as well as Elisabeth P., for their love, encouragement and patience.

Table of Contents

List of Figures

List of Tables

1.0 Introduction

Solid propellant rocket motors are composite structures consisting of a case and a solid propellant grain. The case, or shell, has a relatively simple geometry and can be considered as a thin-walled pressure vessel. The solid propellant grain is the shaped mass inside the case and its geometry may be complicated. In general, the case is made of a stiff elastic material while solid propellant is compliant and viscoelastic. Moreover, the coefficient of thermal expansion of the propellant is several times larger than that of the case. In most motors currently in service, the grain is firmly bonded to the case (case-bonded motors) resulting in a more complex stress analysis of the grain, as well as in several critically stressed areas where multiaxial states of stress hold.

The solid propellant grain has to play two parts simultaneously: it is the source of propulsive energy and is an integral structural component. On one hand, the grain must satisfy some requirements concerning the motor performance (thrust-time profile), the burning rate and the burning surface area. On the other hand, the grain must maintain a structural integrity during handling, storage and rocket operation as it is subjected to static and dynamic loads. More specifically, the solid propellant grain has to meet the high stress concentrations present in case-bonded grain during shrinkage at low temperature as well as

during the dynamic load conditions of ignition and motor operation. The structural integrity of the grain is all the more critical because of the sensitivity of solid propellant grains to cracks and defects. Indeed, during motor operation, cracks and defects may cause an unpredictable and often progressive increase in the burning area and burning rate and thus the failure of the grain. As a result, the assessment of the mechanical and fracture behavior of solid propellants is of a critical importance [1-3].

There are three types of solid propellants: composite, double-base and composite double-base. In this thesis, only composite solid propellants are considered. Composite solid propellants consist of a mixture of stiff inclusions in a soft polymeric binder. These materials are non-homogeneous and behave viscoelastically. Owing to the nature of composite solid propellants, experimental mechanics is widely used to study the behavior of these materials. In the present case, the mechanical and fracture behavior of a simulated composite solid propellant is investigated and the effects of temperature and time are assessed. More specifically, stress relaxation, constant head rate and crack propagation tests have been conducted at various temperatures and head rates.

2.0 Literature Review

2.1 Composite Solid Propellants

2.1.1 Composition

Composite solid propellants consist of a heterogeneous mixture of crystalline oxidizer and powdered metal (fuel) in a soft polymeric binder.

The crystalline oxidizer may represent up to 75% of the propellant by weight. It is chosen based on its performance, compatibility with the other propellant materials, quality and availability. The crystal sizes and size distribution are closely monitored during processing because of their influence on the burning rate. Ammonium perchlorate (NH_4ClO_4) is currently the most widely used crystalline oxidizer. Its good characteristics and the high oxidizing potential of the perchlorates make it suited to high specific impulse propellants.

The prominent solid fuel is powdered aluminum, which represents generally 14 to 18 % of the propellant by weight.

The polymeric binder plays the part of a fuel but more importantly influences the mechanical properties of the grain as well as the reliability of the motor. The relative

proportion of crystalline oxidizer to polymeric binder results from a compromise between the performance of the motor and the mechanical properties of the grain [1].

2.1.2 Physical Properties

Due to the polymeric nature of the binder, composite solid propellants behave viscoelastically; their behavior and properties depend upon time, temperature and the entire past history of deformation. Under small strains these materials can be considered as linear viscoelastic, while under large deformations and in the regions of failure a non-linear description is necessary. Despite their real nature, composite solid propellants are commonly described as macroscopically isotropic and homogeneous. Micro-mechanical studies such as fracture origins must be treated separately [4,5].

2.2 Mechanical Properties of Composite Solid Propellants

2.2.1 Stress Relaxation

In viscoelastic materials, stress relaxation is due to viscous flow and, unlike for ceramics and metals, it can occur at room temperature and even below. The most common way to assess the stress relaxation behavior of viscoelastic materials is to determine their relaxation modulus E_r as a function of time and temperature: $E_r=E_r(t,T)$. Obtaining an accurate description of the relaxation modulus of composite solid propellant following a theoretical procedure often requires long and difficult mathematical considerations. Accordingly, it is generally more convenient to measure the relaxation modulus and then fit the measured data by a specified relation.

The relaxation modulus $E_r(t,T)$ can be determined from constant strain tensile tests conducted at various constant temperatures. This procedure requires an instantaneous specimen extension and the measurement of the diminishing force needed to maintain constant elongation over an extended period of time. The relaxation modulus is computed from the measured data, as follows:

$$E_r(t)=\frac{\sigma(t)}{\varepsilon_o} - R(t) \qquad (2.1)$$

where ε_o is the constant global strain applied on the specimen, $\sigma(t)$ the decreasing stress needed to maintain ε_o, and R(t) a remaining term introduced by the actual ramp time function used to apply ε_o. R(t) has been found to drop out between $t=t_1$ and $t=10t_1$, t_1 being the ramp rise time [2].

The relaxation modulus is commonly described analytically using the modified power law given by:

$$E_r(t)=E_e+\frac{E_g-E_e}{(1+\frac{t}{\tau_o})^n} \qquad (2.2)$$

where:

E_e is the long-time elastic (or rubbery) modulus of the material.

E_g is the short-time (or glassy) modulus of the material.

n is the slope of the relaxation curve (log-log plot) in the transition region between the glassy and the rubbery behavior.

τ_o can be considered as a relaxation time chosen for the best fit of the data.

If one does not consider very small values of t, then $\frac{t}{\tau_o}>>1$, and one can write:

$$E_r(t)=E_o+E_1t^{-n} \qquad (2.3)$$

where $E_o=E_e$ and $E_1=(E_g-E_e)\tau_o^n$.

Figure 2.1 shows a typical relaxation modulus versus time curve obtained for hydrocarbon (HC) propellant. The curve can be divided into three parts. At short and long times the relaxation modulus is constant and equal to E_g and E_e, respectively. These two parts correspond to the glassy and rubbery behaviors of the material. At intermediate times, the relaxation modulus decreases significantly as time increases, dropping from E_g to E_e.

An isochronal plot of the relaxation modulus versus temperature would be similar to the curve shown in Figure 2.1. The maximum temperature below which the relaxation modulus is constant and equal to E_g is the glass transition temperature, T_g, of the material. For composite solid propellants, the glass transition temperature is about -160°F.

2.2.2 Tensile and Ultimate Properties

Constant strain rate tensile tests provide a convenient means to study the viscoelastic properties of composite solid propellants. Tests are commonly conducted under uniaxial or biaxial states of stress and experimental data can be used to derive failure criteria applicable to more general stress states [5,6].

The mechanical response of composite solid propellant is closely related to the strain rate, the temperature and the damage state in the material. Figure 2.2 shows a stress-strain curve for a typical composite solid propellant tested under a constant strain rate. The dewetting strain ε_d is, by definition, the strain (and corresponding stress) at which incipient failure of the interfacial bond between oxidizer particles and the binder occurs. Below ε_d the curve is

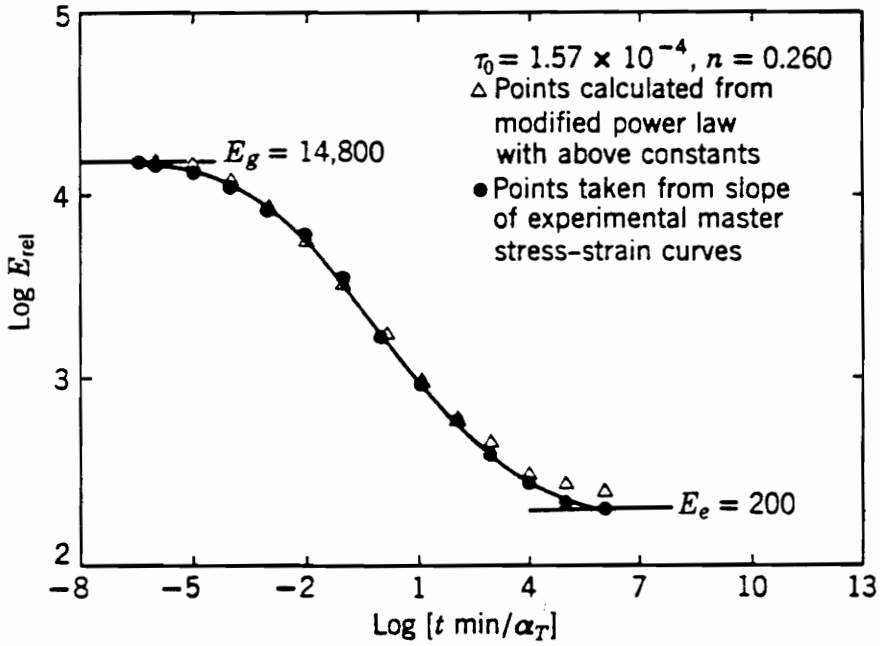

Figure 2.1. Typical Relaxation Modulus Curve for HC Propellant [4].

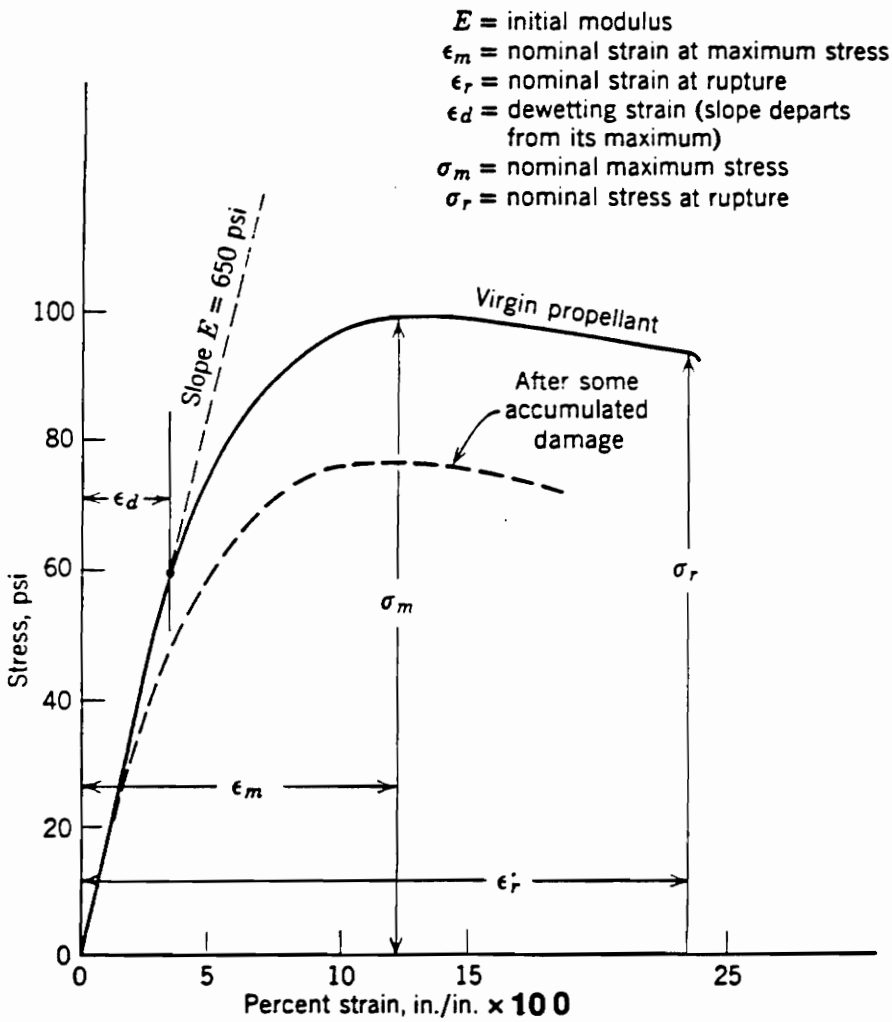

Figure 2.2. Stress-Strain Curve for a Typical Composite-Type Propellant [1].

essentially linear and is associated with the stretching of the undamaged material, i.e., the oxidizer particles (or filler particles) are bonded to the binder. Above ε_d the material is significantly damaged and the stress-strain curve is highly non-linear. The debonding (or dewetting) process taking place in the material above ε_d will be discussed in more detail in a subsequent section.

Figure 2.2 is in fact a simplification of the actual behavior of composite solid propellant. Indeed, a close observation of the stress-strain curve of a typical composite solid propellant tested under constant strain rate generally reveals no linear zone, even at small strains [7]. However, Figure 2.2 provides a very convenient means to introduce the dewetting strain ε_d.

2.2.3 Time and Temperature-Dependent Mechanical Behavior

2.2.3.1 Time-Temperature Superposition Principle for Polymers

The early work on the time-temperature equivalence was done studying the relaxation modulus of polymers as a function of time and temperature. A shifting procedure has been found to enable one to construct a master curve showing the complete modulus-time behavior at constant temperature. This procedure is based upon the time-temperature superposition principle, which can be described as follows.

Let one consider two temperatures T_1 and T_2. The time-temperature superposition principle is mathematically expressed as:

$$E_r(T_1,t)=E_r(T_2,\frac{t}{a_T}) \qquad (2.4)$$

where $\frac{t}{a_T}$ is the temperature-reduced time variable.

In other words, data obtained at one temperature can be superimposed to that obtained at another temperature by applying a multiplicative factor to the time scale, i.e., an additive factor to the log time-scale. The time-temperature superposition principle has been found to be extremely successful for a large variety of amorphous polymers, even though it is quantitatively correct over limited time-temperature ranges [8,9]. Through its application, the curves obtained at various temperatures can be shifted horizontally along the log(t) axis to yield a master curve at a particular temperature, as shown in Figure 2.3.

The time-temperature superposition principle can be applied to other mechanical properties of polymers, such as initial Young's modulus and ultimate properties. These mechanical properties are determined during constant strain rate tensile tests conducted at various temperatures and can be superimposed using the temperature-reduced strain rate variable $\dot{\varepsilon}a_T$.

The time-temperature superposition principle is useful in predicting the mechanical behavior of polymers outside the ranges of time and strain rate for which experimental data are available. As a result, it is a convenient means to study the mechanical behavior of polymers from their glassy to their rubbery state [10].

Williams, Landel and Ferry [11] investigated the effects of time and temperature on the relaxation properties of polymers and came up with a mathematical model for the shift factor $\log(a_T)$. The relationship proposed by Williams, Landel and Ferry, known as the WLF equation, is as follows:

$$\log(a_T) = \frac{-C_1(T-T_0)}{C_2+T-T_0} \qquad (2.5)$$

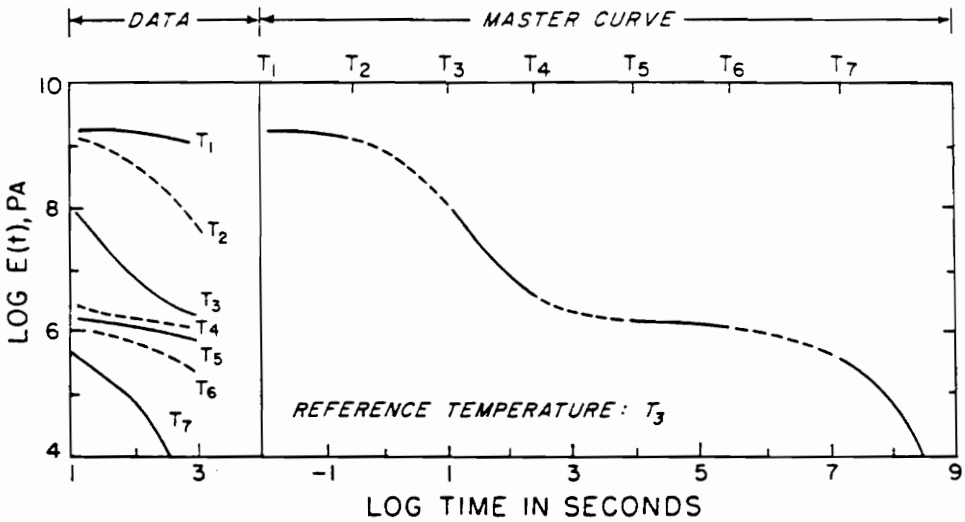

Figure 2.3. Preparation of a Stress Relaxation Master Curve from Experimentally Measured Modulus-Time Curves at Various Temperatures [8].

where C_1 and C_2 depend only upon the reference temperature T_0. C_1 and C_2 are generally determined by fitting equation (2.5) to the experimental data.

Although the WLF equation was developed experimentally by curve fitting, it is possible to justify it theoretically based on consideration of the free volume [10,12].

2.2.3.2 Application of the Time-Temperature Superposition Principle to Composite Solid Propellants

The proportion of polymeric binder in composite solid propellants is relatively small and these materials are strongly influenced by the presence of the filler particles. However, the application of the time-temperature superposition principle to composite solid propellants has been successful and has found general acceptance in the industry. For some propellants, there is evidence for the necessity of a vertical shift in addition to the aforementioned horizontal shift [5-7].

2.3 Failure of Composite Solid Propellants

2.3.1 Failure Mechanism

The assessment of composite solid propellant failure mechanism requires one to study the material on a microscopic scale. As a result, solid propellant is considered as non-homogeneous and the interactions between the hard filler particles and the soft polymeric binder are highlighted.

Failure of composite solid propellants may be initiated in two different ways. Initiation of failure may be due to the separation of the binder from the filler particles (dewetting) or, if the binder-filler bond strength exceeds the strength of the binder itself, initiation of failure

may take place within the binder. Owing to the nature and physical properties of composite solid propellants, the failure process of these materials is complex and involves a number of factors, among which dewetting is probably the most important.

Dewetting is generally the first step of composite solid propellant fracture. It occurs first on a microscopic scale and depends primarily upon the adhesive bond between the binder and the oxidizer particles. Dewetting requires a critical stress to be reached to initially cause failure of an oxidizer-binder bond, after which it propagates to the neighboring particles, producing a dewetted band or region. The dewetted regions are relatively weak and provide the sites for future failure of the propellant. Once dewetting occurs, a tearing is initiated in the binder at locations of stress concentration such as regions of binder-oxidizer dewetting. Dewetting behavior depends upon both time and temperature and it can be divided into four classes:

- class 1: essentially complete dewetting occurs prior to fracture.
- class 2: dewetting occurs in two or more bands as well as in local sites throughout the specimen.
- class 3: dewetting occurs in a small area only.
- class 4: no dewetting occurs prior to fracture.

As temperature decreases and strain rate increases, the dewetting character shifts from class 1 to class 4. As a result, at high temperature and low strain rate (class 1 and 2 behavior) the failure tends to be of a ductile nature, whereas at lower temperatures and higher strain rates (class 3 and 4 behavior) failure is a brittle-type fracture.

Most of the composite solid propellants currently used are of class 1 or 2 and fall to class 3 and 4 below 0°F. For classes 1 to 3, a study of failure using a strain energy approach is of interest, whereas for class 4 the classical theory of elasticity holds quite well .

Failure criteria must take into account the effects of time and temperature. Accordingly, brittle fracture theory can be used for high strain rate and low temperature conditions; tear

theory is used for high temperature and low strain rate conditions. A combination of brittle fracture and tear theories can be used for intermediate conditions [6].

2.3.2 Crack Propagation in Composite Solid Propellants

Linear viscoelastic and elastic fracture mechanics theories have been successfully used in characterizing the crack growth behavior in some propellants.

2.3.2.1 Physical Description

In composite solid propellant, as a crack opens and propagates, the material surrounding the crack tip can be divided into two regions: a failure process zone and an undamaged region. As shown in Figure 2.4, the failure process zone consists of damaged material and generally develops behind the crack tip. Its behavior may be highly non-linear and is widely influenced by the local microstructure and strength of the material. The damage in the failure process zone is in the form of microvoids or microcracks in the binder or in the form of dewetting between the binder and the filler particles. More specifically, the failure process zone consists of a large number of small voids separated by strands of filled rubber. As the applied tensile strain increases, the voids coalesce due to the fracturing of the strands. The failure process zone is generally cusp-shaped and strongly influences the crack propagation. Due to the viscoelastic nature of the binder, the damage initiation and evolution processes are time-dependent, leading to a time-dependent crack growth behavior [13,14].

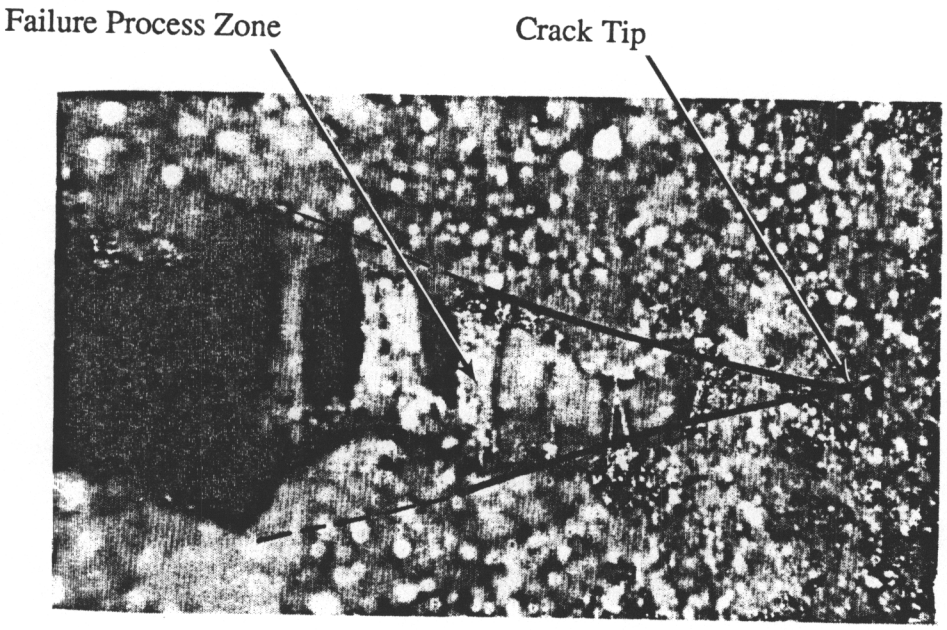

Figure 2.4. Crack in Solid Propellant [16].

Outside the failure process zone, the material is undamaged and behaves linearly up to a critical value of applied strain. Above this threshold value, the material outside the failure process zone is significantly damaged and becomes highly non-linear [15].

As long as it can be divided into a failure process zone and an undamaged region, the near tip region is similar to the model developed by Schapery for linear and isotropic viscoelastic materials [16-18]. In such a case, the mathematical model developed by Schapery for continuous crack growth in linear and isotropic viscoelastic materials is expected to hold for composite solid propellants. Figure 2.5 shows the crack tip model used by Schapery, in which the crack tip is located at the right end of the failure process zone.

2.3.2.2 Mathematical Description

Highly filled composite solid propellants are, on the microscopic scale, non homogeneous. The local behavior depends strongly on the degree of cross linking of the matrix material, the filler particles size and distribution, and the bond strength at the interface of the filler particles and the matrix. As a result, the local stresses and strength vary randomly and the failure may not occur at the location where the local stress reaches a maximum [14]. This inherent non homogeneous nature of composite solid propellants inevitably causes a large scatter in the measured data (applied load, crack length and time). Consequently, a statistical analysis of the experimental data is desirable.

The combination of statistical analyses with the mathematical model developed by Schapery leads to a very good agreement between theoretical and experimental results. Accordingly, for many propellants [19-23], the experimental data yield a power law relationship between the crack growth rate and the mode I stress intensity factor:

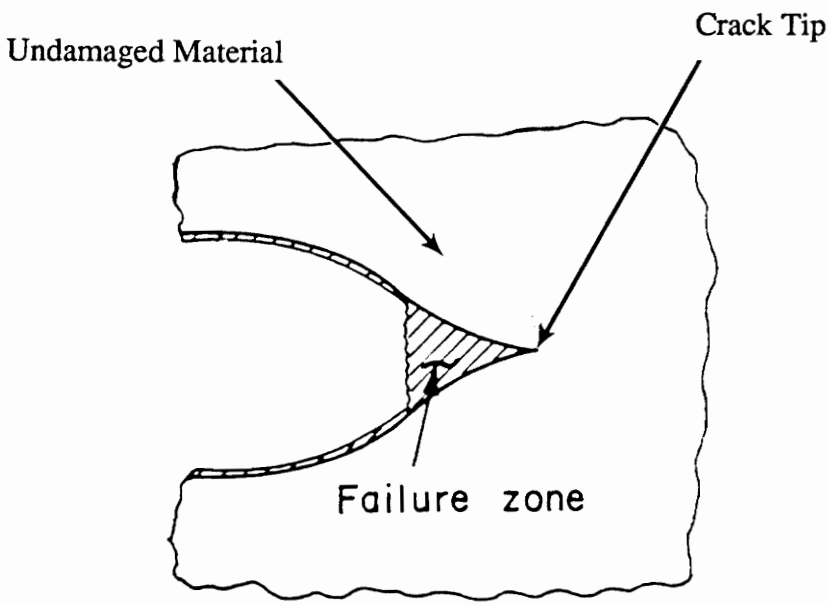

Figure 2.5. Cross-Section of an Idealized Crack [16].

$$\dot{a} = \frac{da}{dt} = AK_I^q \qquad (2.6)$$

where:

$\dot{a}$ = crack tip velocity.

K_I = mode I stress intensity factor.

Theoretically, A and q are two constants and q is determined by the creep compliance. However, for some composite solid propellants, A and q are not constant, but are mutually dependent and related through a simple equation given by:

$$\log A = B + Cq \qquad (2.7)$$

where B and C are constants.

The existence of a good correlation between the crack growth rate and the instantaneous mode I stress intensity factor indicates that the crack growth behavior is controlled by the local stress near the crack tip.

2.4 Dominant Eigenvalues at the Crack Tip

In 1975, Benthem started the three dimensional analysis for stress and displacement eigenvalues determination in the region where a straight crack front intersects a free surface. As shown in Figure 2.6, he used a spherical coordinate system (r,θ,ϕ) to study the case of a quarter-infinite crack in a half space. The half space extended along $\theta \leq \frac{\pi}{2}$ and the crack was located along $\phi=0$. His objective was to determine the dominant stress eigenvalue (or stress singularity order) λ_σ and the corresponding state of stress at the point

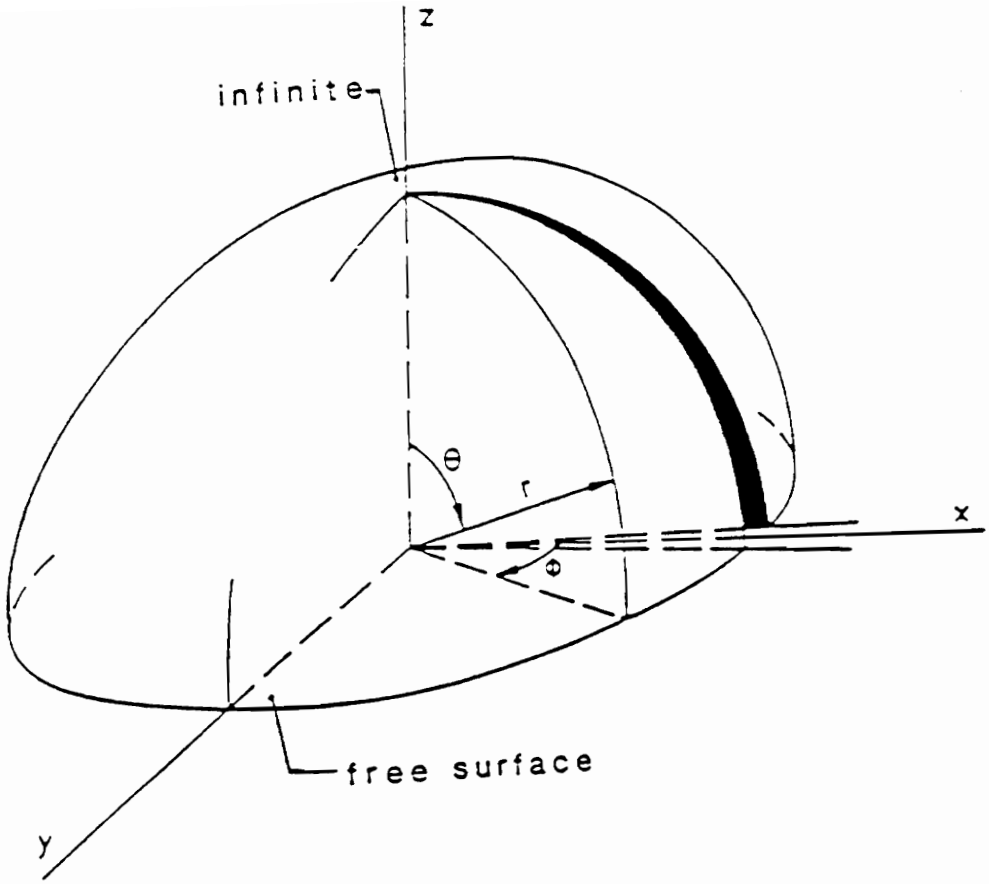

Figure 2.6. Geometry Used by Benthem [24].

where the straight crack front intersects the free surface at right angle. He used the Papkovich-Neuber stress functions to solve the Navier-Cauchy displacement field equations. In [24, 25] he used a separation of variables technique to study symmetrical states of stress and formulated the stresses and displacements as follows:

$$\sigma_{ij} = r^{\lambda_\sigma^k} f_{ij}^k(\theta,\phi) \qquad (2.8)$$

$$U_i = r^{\lambda_u^k} h_i^k(\theta,\phi) \qquad (2.9)$$

where λ_σ^k and λ_u^k are the stress and displacement eigenvalues and f_{ij}^k and h_i^k are the stress and displacement eigenfunctions, respectively. In [26], he used a finite difference technique to confirm the results of [24, 25] and to investigate anti-symmetrical states of stress.

Benthem showed that in the neighborhood of the origin or vertex, the state of stress was essentially three-dimensional. This means that two dimensional analyses based on plane strain as well as the concept of stress intensity factor are invalid near the free surface. He also noticed that the inverse square root stress singularity was lost in this region. Finally, he showed that the stress singularity order at the free surface was dependent upon Poisson's ratio. This dependency is shown in Figure 2.7. The greatest difference in stress singularity from the value of -0.5 occurs (for real materials) when Poisson's ratio is one-half, i.e., the material is incompressible. In this case, the stress singularity order, λ_σ, at the free surface is -0.33 and the dominant displacement eigenvalue, λ_u, is $\lambda_\sigma+1= 0.67$.

Benthem's analytical solution for three-dimensional crack problem and numerical verification have been generally accepted in the fracture mechanics community. This work shows that the free surface does influence the stress singularity order and that the so-called surface effect is more pronounced at higher values of Poisson's ratio than that for common engineering materials.

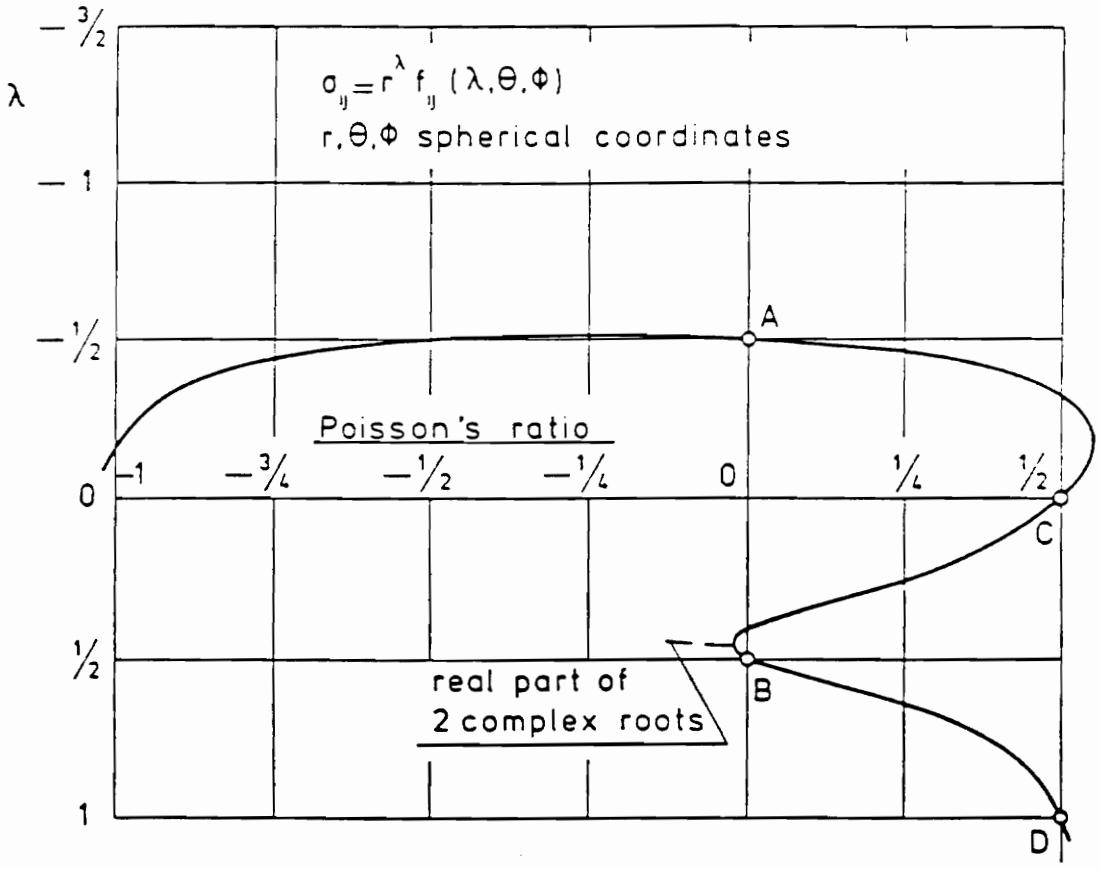

Figure 2.7. Benthem's Result on Stress Singularity at the Free Surface [24].

3.0 Experimental Procedures

3.1 Material

The specimen material is a simulated composite solid propellant whose composition is given in Table 3.1. The word simulated refers to the fact that the basic ingredients of live composite solid propellant are kept, except that the oxidizer particles of ammonium perchlorate may be replaced by other crystals. Figure 3.1 shows a micrograph of the material. The crystals are observed to be uniformly distributed and their size ranges from 0.001 to 0.3 mm.

3.2 Grid Method

The most important consideration in the near tip measurements is to use a method which does not stiffen the material response. Although normally used for large strain measurements, the grid method was chosen for the following reasons:

i) The grid has a negligible stiffness.

ii) Controllable pitch can be selected to bring out desired features.

Table 3.1. Typical Composition of Composite Solid Propellant [1].

Ingredient	Weight %
Ammonium perchlorate*	70.0
Aluminum powder	16.0
Polybutadiene- acrylic acid- acrylonitrile	11.78
Epoxy curative	2.22

*: In simulated composite solid propellant the oxidizer particles of ammonium perchlorate may be replaced by other crystals.

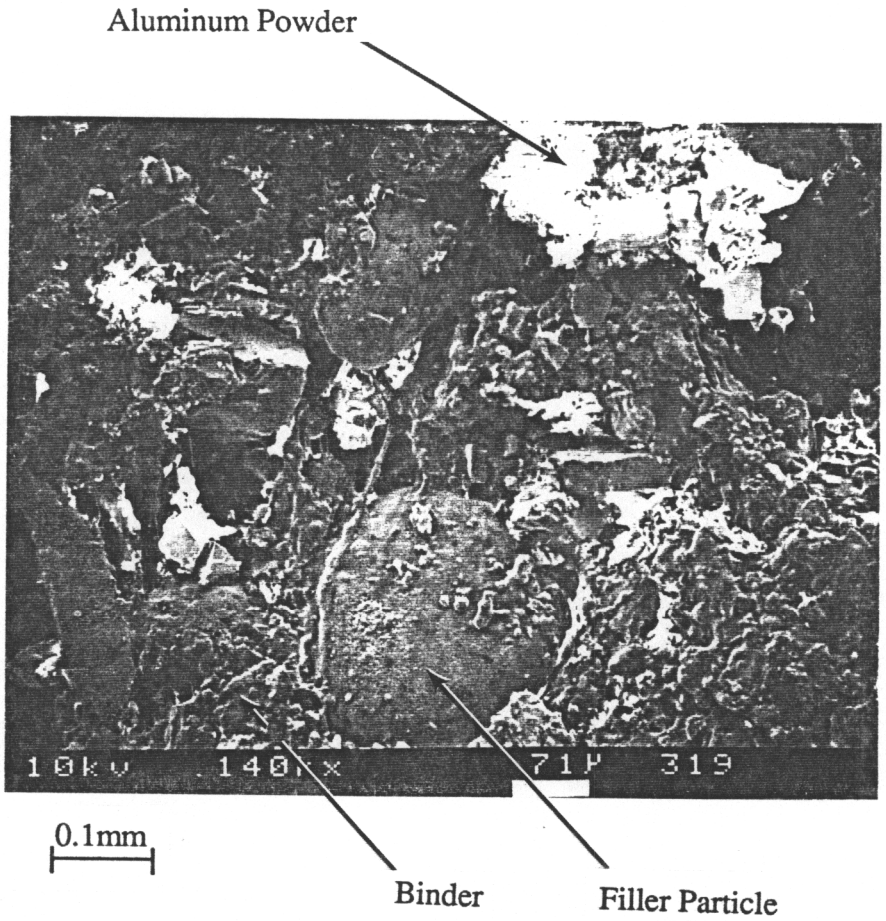

Figure 3.1. Micrograph of the Material (Magnification Factor: 140).

iii) Surface damage is easily delineated.

iv) A continuum interpretation is possible.

In any case, the method must be a compromise which emphasizes features of interest, since no large strains are recorded.

The grid method consists of applying a grid to the surface of the specimen and measuring the distance between discrete points on the grid both before and after deformation. The subsequent analysis of these measurements consists of determining the displacements of selected points and then deriving the strains from the displacements. A Lagrangian description or the infinitesimal-deformation theory is commonly used for strain-displacement relations. The use of the latter requires only the in-plane displacements U and V to compute the in-plane strains ε_{xx}, ε_{yy} and ε_{xy}, which leads to valid results up to a strain level of 15%. The use of a Lagrangian description gives results valid up to a higher strain level but requires the determination of out-of-plane displacement W [27].

The grid method has been found to be very useful in measuring the in-plane displacements and large local strains in the near crack tip region. Moreover, the grid method is well suited to the study of crack propagation in composite solid propellants. It is indeed sufficiently refined for near tip studies, yet coarse enough to smooth out the highly local irregularities due to the rigid filler particles [28].

3.3 Specimen Geometry and Preparation

3.3.1 Specimen Geometry

The mechanical and fracture behavior of composite solid propellant is commonly assessed using a biaxial strip specimen. The specimen is restrained in one dimension while tensile strained in a second and allowed to deform freely in the thickness. The lateral restraint is

generally provided by bonding the specimen at the upper and lower edges to holders, which, to a fair extent, prevents lateral contraction of the specimen. As a result, a biaxial state of strain holds at the center of the specimen. Since composite solid propellant is nearly incompressible, the resulting state of stress is a two-dimensional biaxial tension. Figure 3.2 shows a biaxial strip specimen and the biaxial state of stress at its center.

The biaxial strip specimen is widely used to study the mechanical and fracture behavior of composite solid propellant because it is considered to be a good approximation of the biaxial state of strain met at the inner bore of a fully case-bonded grain [6,7].

3.3.2 Specimen Preparation

3.3.2.1 Uncracked Biaxial Specimen

Figure 3.3 (a) shows the uncracked biaxial specimen. Circular cutouts were made on the sides of the specimen in order to prevent premature failure of the strip specimen at the grips. Then, the specimen was cemented into rigid aluminum grips.

3.3.2.2 Pre-Cracked Biaxial Specimen

Figure 3.3 (b) shows the pre-cracked biaxial specimen. One end of the specimen was rounded in order to prevent premature failure at the grips. At the other end a straight crack of initial length a_0 was inserted. Insertion of the crack was very critical and care was taken to assure a sharp crack tip. Two guides and a knife were used. The sides of the knife were sharpened to give a sharp crack tip; the guides directed the knife into the specimen, resulting in a sharp and straight crack. The length of the initial crack was about 23 mm.

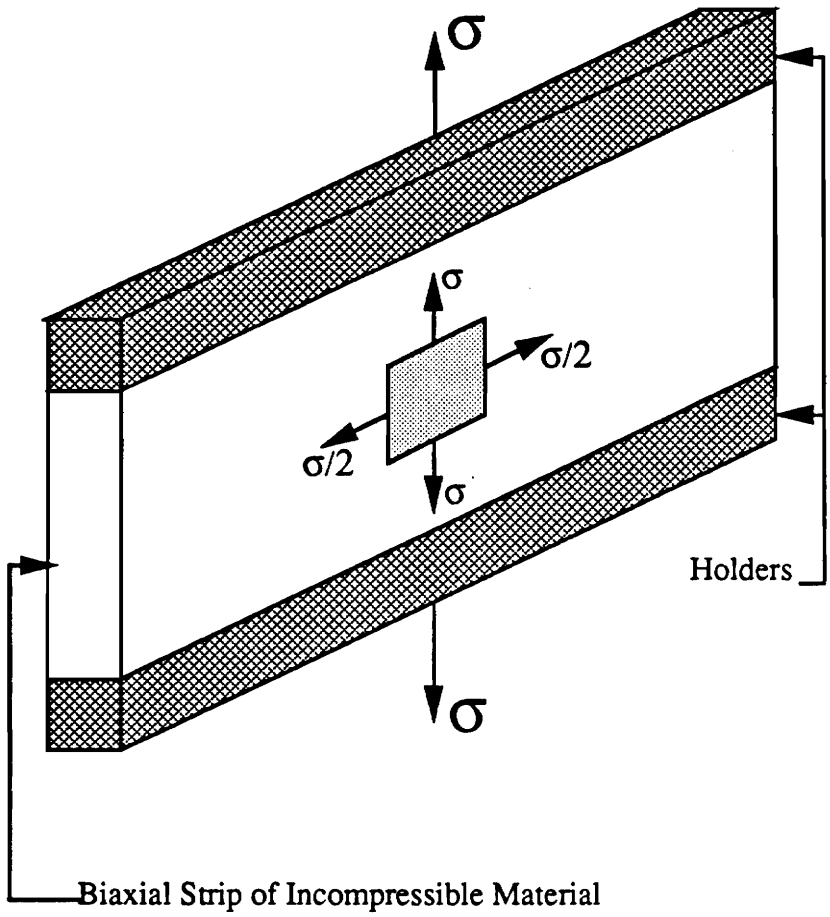

Figure 3.2. Biaxial Strip Specimen.

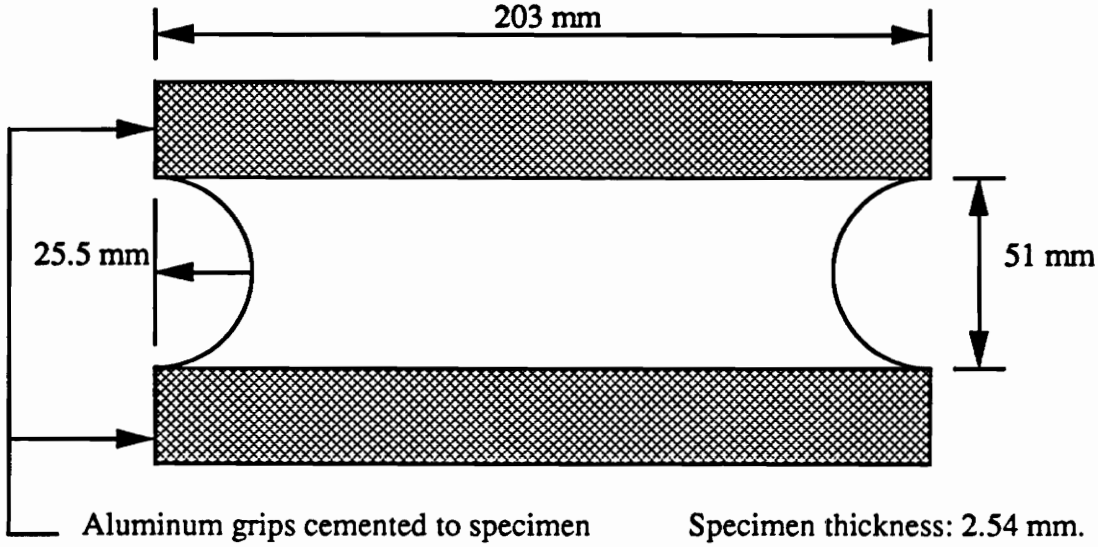

(a) Uncracked Biaxial Specimen

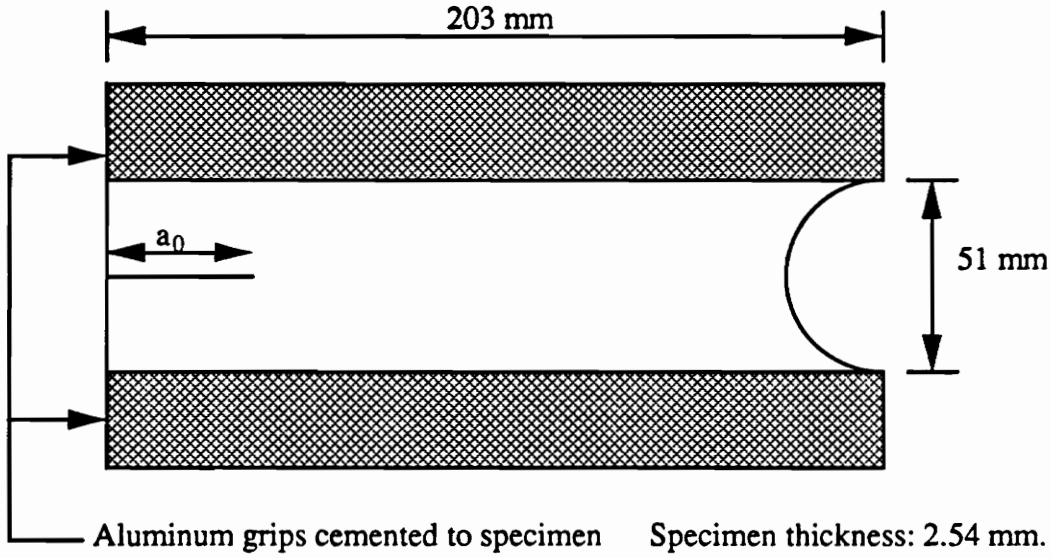

(b) Pre-Cracked Biaxial Specimen

Figure 3.3. Test Specimens.

The next step consisted of transferring a grid to the surface near the crack tip. Considering earlier experiments conducted on a similar material [29], the pitch of the grid was chosen to be 0.2 mm. This choice was motivated by the desires to obtain an average effect of the large filler particles and to apply continuum theory to the results.

In order to achieve accurate surface displacement measurements without stiffening the specimen, the grid was applied to the surface as follows:

- Apply a mixture of silicone vacuum grease and titanium dioxide powder to the surface near the crack tip.
- Place a thin metal mesh on the mixture with one set of lines carefully aligned with the direction of the crack.
- Remove the excess of mixture.
- Evaporate aluminum over the surface (the mesh was used as a mask).
- Remove the metal mesh.

Aluminum turned black when evaporated onto the silicone grease and the final result was a cross-grating of white lines on a black background. The total thickness of the grid was less than 2.5 10^{-2} mm.

Finally, the specimen was cemented to aluminum grips using a fast setting epoxy.

Figure 3.4 shows a picture of the grid transferred to the surface of the region surrounding the crack tip.

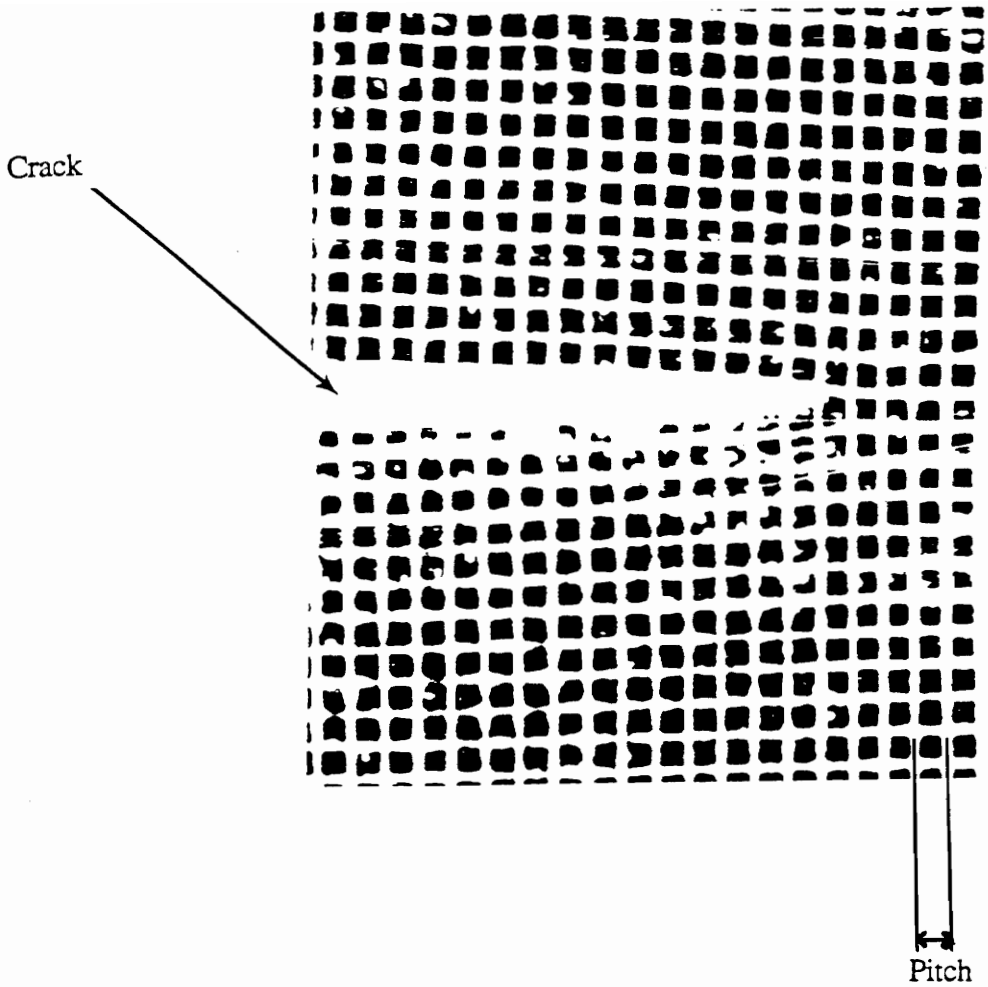

Figure 3.4. Picture of the Grid Transferred to the Surface Surrounding the Crack Tip.

3.4 Testing Conditions

The viscoelastic nature of composite solid propellants requires their mechanical and fracture behavior to be assessed as a function of temperature and time (or strain rate). As a result, three temperatures and two head rates were considered.

Stress relaxation tests, constant head rate tensile tests, and crack propagation tests were conducted at -65°F, room temperature (72°F) and 165°F. For the tests conducted at -65°F and 165°F, the specimens were set up in a conditioning cabinet first and then the temperature was decreased or increased.

For the tests conducted at -65°F, the cooling was done using liquid nitrogen. The cooling process was divided into two stages. First, the temperature in the conditioning cabinet was decreased from room temperature to -65°F in about 40 minutes. Second, the temperature was maintained constant for 15 minutes prior to the test as well as during the test. During the cooling process the specimens shrank and were under a small amount of tension.

For the tests conducted at 165°F, the heating process was very similar to the cooling process previously described. The temperature in the conditioning cabinet was increased from room temperature to 165°F in about 30 minutes. Then, the temperature was maintained constant for 15 minutes prior to the test and during the test.

All the specimens were loaded in tension by translation of the upper grip. The constant head rate tensile tests were conducted under a head rate of 2.54 mm/min., while the crack propagation tests were conducted under two different head rates: 2.54 and 12.7 mm/min. For the stress relaxation tests, a global strain of 3% was applied using a head rate of 127 mm/min. The loading time was roughly one second. All the tests were duplicated and the results were averaged.

3.5 Data Collection and Reduction

3.5.1 Stress Relaxation Tests

During the stress relaxation tests, the decreasing load required to maintain constant applied global strain was recorded as a function of time. This load was then converted into stress and relaxation modulus using the following equation:

$$E_r(t) = \frac{\sigma(t)}{\varepsilon_o} \qquad (3.1)$$

where ε_o is the applied global strain.

The stresses were computed based on the average initial cross-section of the specimens.

3.5.2 Constant Head Rate Tensile Tests

During the constant head rate tensile tests, the load versus time curves were recorded and converted into stress-strain curves. As for the stress relaxation tests, the stresses were computed based on the average initial cross-section of the specimens. The strains were determined as follows:

$$\varepsilon = \frac{\delta}{L_0} 100\ \% \qquad (3.2)$$

where δ is the upper grip displacement and L_0 the initial height of the specimens.

3.5.3 Crack Propagation Tests

For each test, the data were recorded in the form of pictures of the grid and in the form of a printout of the load versus time curve. Pictures were taken both before and during stretching of the specimen, using a 35mm camera. For the tests conducted at room temperature, the crack propagation was also videotaped. Pictures were used to study the deformation of the grid and the crack propagation process. Selected exposures were printed to determine the dominant displacement eigenvalue at the free surface as well as the displacement and strain fields near the crack tip. Figure 3.5 shows the set-ups used to observe the crack propagation and take pictures of the grid. The direction of incident light was observed to be critical for the quality of the pictures.

3.5.3.1 Study of the Crack Propagation Process

From the pictures, the crack length was determined as it varied with time. When possible, the amount of blunting of the crack tip and the size of the failure process zone were determined as well.

3.5.3.2 Determination of the Displacement and Strain Fields at the Free Surface in the Near Tip Region

For each test, the V displacement field, ε_{yy} and ε_{xy} strain fields in the near tip region were determined both before and after crack propagation (the X-axis lies in the crack plane while the Y-axis is normal to the crack plane. The origin is located at the crack tip). To do so, pictures of the grid taken prior to and during stretching were used. On each picture,

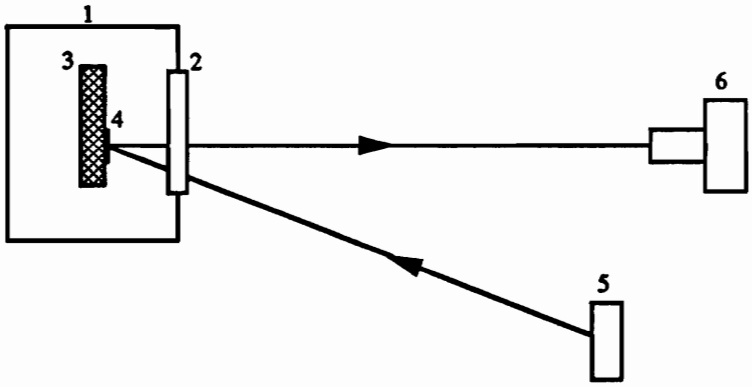

1: conditioning cabinet
2: window
3: specimen
4: grid
5: light source
6: 35 mm camera with lens

(a) Observing Set-Up Used for the Crack Propagation Tests Conducted at -65°F and 165°F

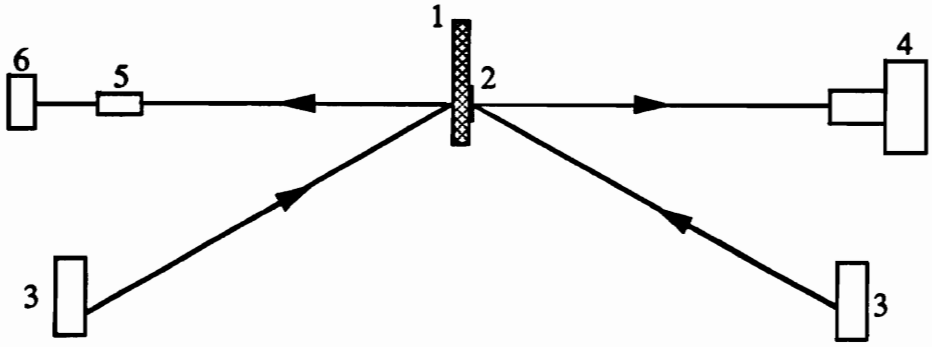

1: specimen
2: grid
3: light sources
4: 35 mm camera with lens
5: microscope
6: video

(b) Observing Set-Up Used for the Crack propagation Tests Conducted at Room Temperature

Figure 3.5. Grid and Crack Propagation Observing Set-Ups.

selected lines of the grid were marked and the points located at the intersections of these horizontal and vertical lines were digitized. A separate computer program was used for data analysis. The data reduction technique was designed to attenuate extensive small-scale irregularities due to the stiff filler particles so that the contours of displacements and strains show general trends. This computer program performed the following operations:

- Subtraction of the coordinates of the undeformed grid from that of the deformed grid, to obtain the U (horizontal) and V (vertical) displacements corresponding to the loading condition.
- Derivation of the in-plane strains from the in-plane displacements. This was done using the infinitesimal-deformation theory.
- Plotting the contour maps of the displacements and strains.

More details on this method are given in references [30,31].

3.5.3.3 Determination of the Dominant Displacement Eigenvalue at the Free Surface

The dominant displacement eigenvalue λ_u was determined at the point where the crack front intersected the free surface, as follows.

On the pictures taken during stretching, a straight line passing through the crack tip and normal to the crack plane was drawn. The intersections of this line with the deformed horizontal lines of the grid were chosen as data points. Using a digitizing table and a personal computer, the coordinates of the data points were recorded. The corresponding displacements were computed by subtracting the initial coordinates of the data points from their coordinates after deformation. Data were collected both above and below the crack tip and were then averaged. The dominant displacement eigenvalue λ_u where the crack front intersected the free surface at right angle was subsequently determined as follows.

By truncating equation (2.9) for the displacement $V=U_2$, one may write for $\phi=\theta=\frac{\pi}{2}$ (see Figure 2.6):

$$V=Ar^{\lambda_u} \qquad (3.3)$$

whence:

$$\ln(V)=\ln(A)+\lambda_u\ln(r) \qquad (3.4)$$

where A is a constant and r is the distance from the measured point to the crack tip.

As a result, since the free surface displacement components V are known, one can determine the dominant displacement eigenvalue λ_u from a plot of ln(V) versus ln(r).

4.0 Results and Discussion

4.1 Material Characterization

4.1.1 Stress Relaxation Tests

The diminishing load required to maintain the applied global strain of 3% on the specimens was recorded from t=3 seconds to t=1 hour and was then used to determine the relaxation modulus. Figure 4.1 shows the curves of the relaxation modulus E_r versus t for the three temperatures considered. These curves were obtained by curve fitting of the experimental data. The general form of the equation $E_r(t)$ versus t is as follows:

$$E_r(t)=E_0+E_1t^{-n} \qquad (4.1)$$

The values of E_0, E_1 and n for the three temperatures considered are given in Table 4.1. Over the range of temperatures investigated, E_0 and n are constant and are respectively equal to 0.98 N/mm^2 and 0.32.

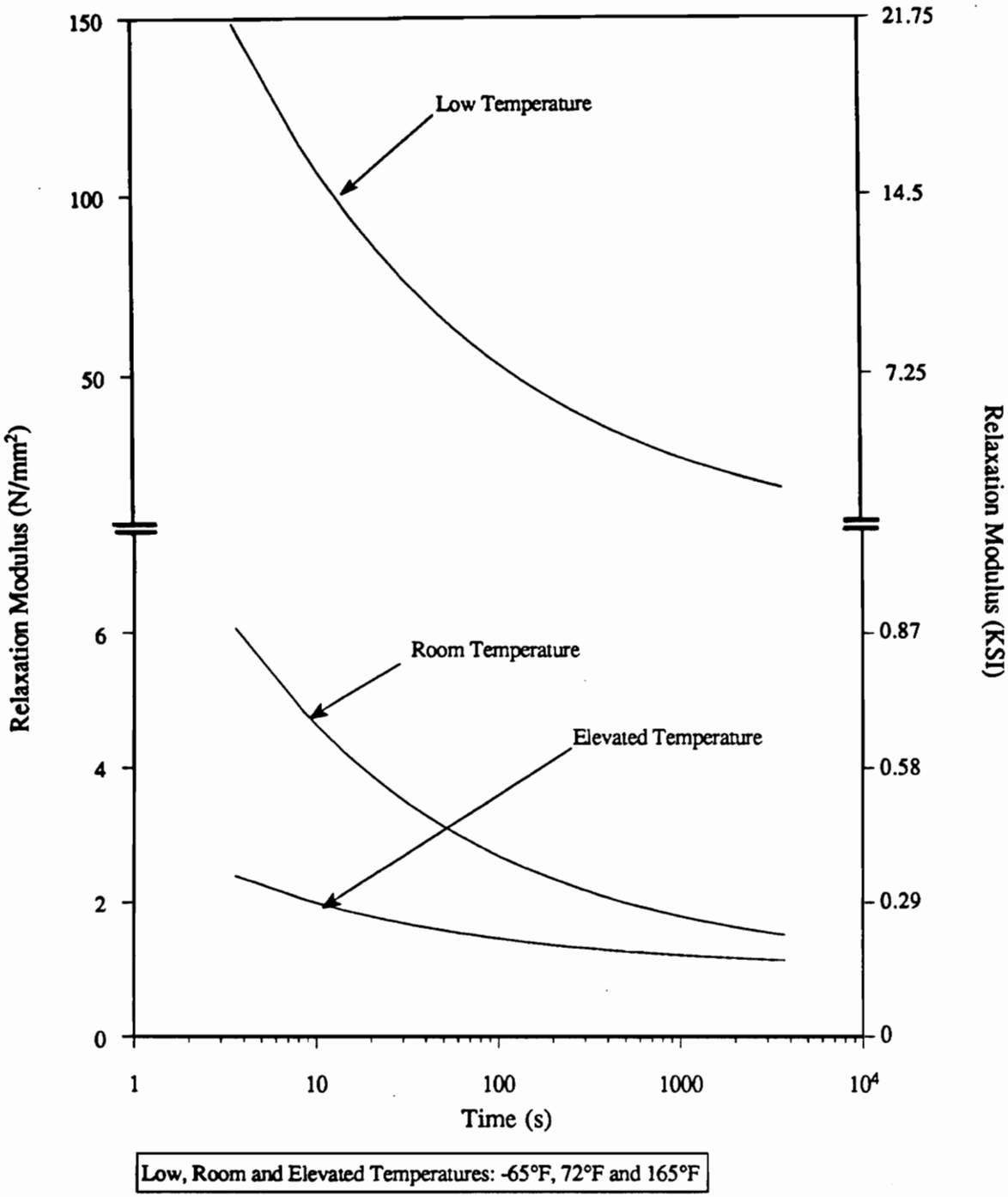

Figure 4.1. Relaxation Modulus versus Time at -65°F, 72°F and 165°F.

Table 4.1. Coefficients E_0 and E_1 and Exponent n of Equation (4.1).

Temperature (°F)	E_0 (N/mm^2)	E_1 (N/mm^2)	n
-65	0.98	220	0.31
72	0.98	7.73	0.33
165	0.98	2.14	0.32

The superposition of the curves obtained at -65°F and 165°F to that obtained at room temperature results in the master curve shown in Figure 4.2. The shift factors $Log_{10}a_T$ (see equations 2.4 and 2.5) used to perform the superposition were determined experimentally as:

T= -65°F (219°K): $Log_{10}a_T$= 4.54

T= 165°F (347°K): $Log_{10}a_T$= -1.74

The WLF equation, given by equation (2.5), was then fitted to the experimental data $log_{10}a_T$ versus T. Considering T_0 to be 72°F (295 °K), the curve fitting led to the following values of C_1 and C_2:

C_1= 9.78

C_2= 240 °K.

As a result, equation (2.5) reduces to:

$$log_{10}a_T = \frac{-9.78(T-T_0)}{240+T-T_0} \qquad (4.2)$$

Figure 4.3 shows the experimental data points and the WLF curve corresponding to equation (4.2).

The relaxation data show a well defined behavior, following the time-temperature superposition principle. Moreover, the WLF equation seems to be suited to describe analytically the shift factor $log_{10}a_T$ as a function of temperature.

As expected, in the ranges of time and temperatures considered, the relaxation modulus of the material depends strongly upon time and temperature. Since no glassy behavior was observed, the glassy modulus E_g couldn't be determined. By way of contrast, the rubbery modulus E_e could be determined and was found to be equal to 0.98 N/mm^2. The comparison between the curves shown in Figures 2.1 and 4.2 indicates that the ranges of

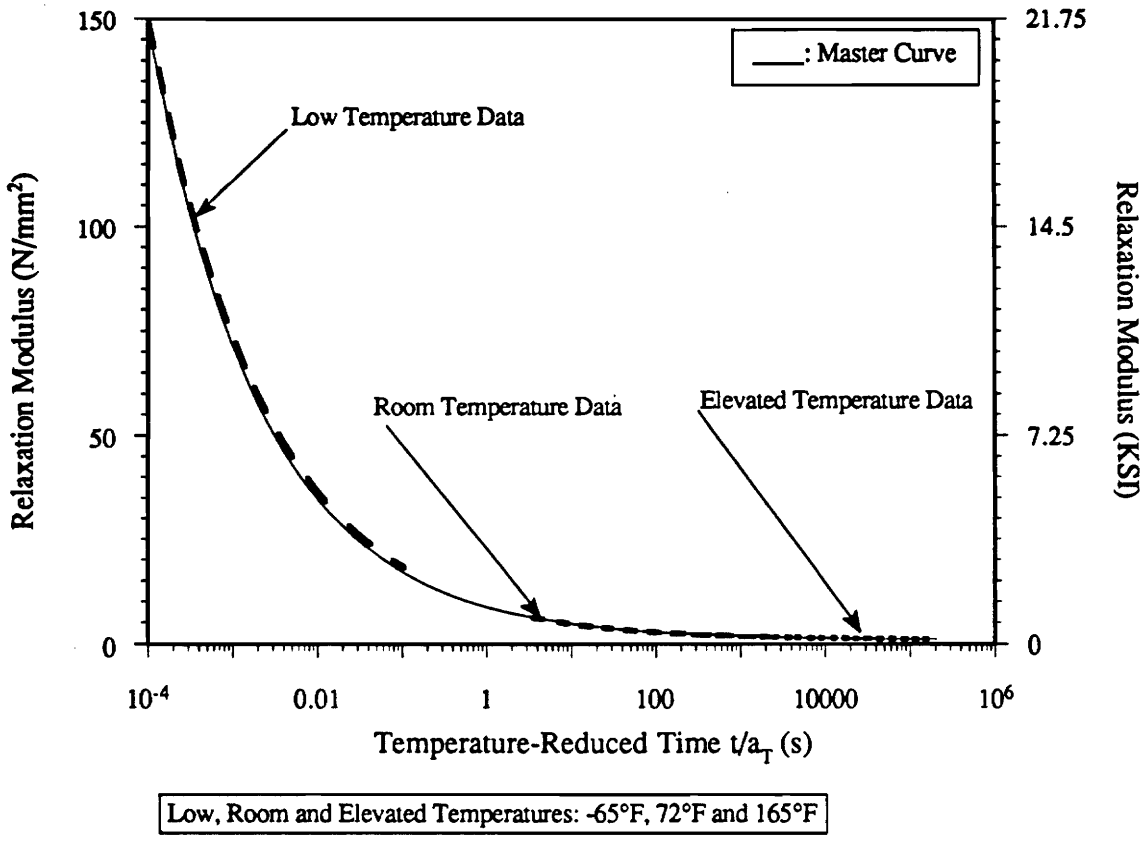

Figure 4.2. Master Curve of the Relaxation Modulus at Room Temperature (72°F).

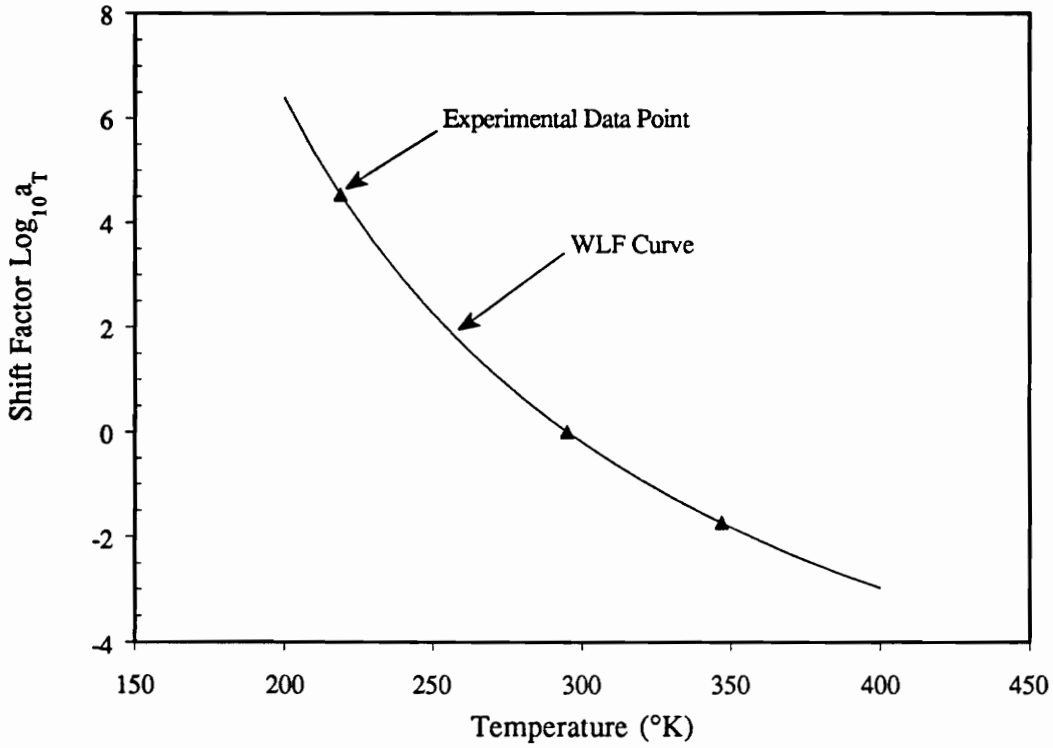

Figure 4.3. Shift Factor versus Temperature.

time and temperatures considered in the present case correspond to the transition region, in which the behavior of the material changes from glassy to rubbery.

4.1.2 Constant Head Rate Tensile Tests

Figure 4.4 shows the stress-strain curves obtained at low, room and elevated temperatures, for a constant head rate of 2.54 mm/min. The curves can be divided into three parts. First, the stress increases monotonically until it reaches a maximum. Then it remains constant for a while and finally drops. The length of the plateau and the shape of the stress-strain curves in the region of declining were observed to vary from test to test. These two features were believed to depend more upon the way the specimen failed (such as failure near the grips or in the center plane of the specimen) than upon the temperature-dependent behavior of the material. As a result, only the first part of each curve was studied. The curves obtained at low and room temperatures are smooth all the way to fracture, with a continuously decreasing slope. At elevated temperature the curve exhibits the sigmoid shape characteristic of rubber-like materials. None of the curves show any linear behavior, even at small strains.

The stress-strain curves reflect the viscoelastic behavior of the material as well as its failure. In other words, the smoothness and continuously decreasing slope of the curves obtained at low and room temperatures are the result of the processes of stress relaxation and dewetting taking place in the material at the same time as the specimens are stretched. The sigmoid shape observed at elevated temperature indicates a qualitative change in the behavior of the material due to temperature. However, except in a small region, the stress-strain curve at elevated temperature can be described in the same way as the curves corresponding to low and room temperatures. In reference [1] Sutton showed the stress-

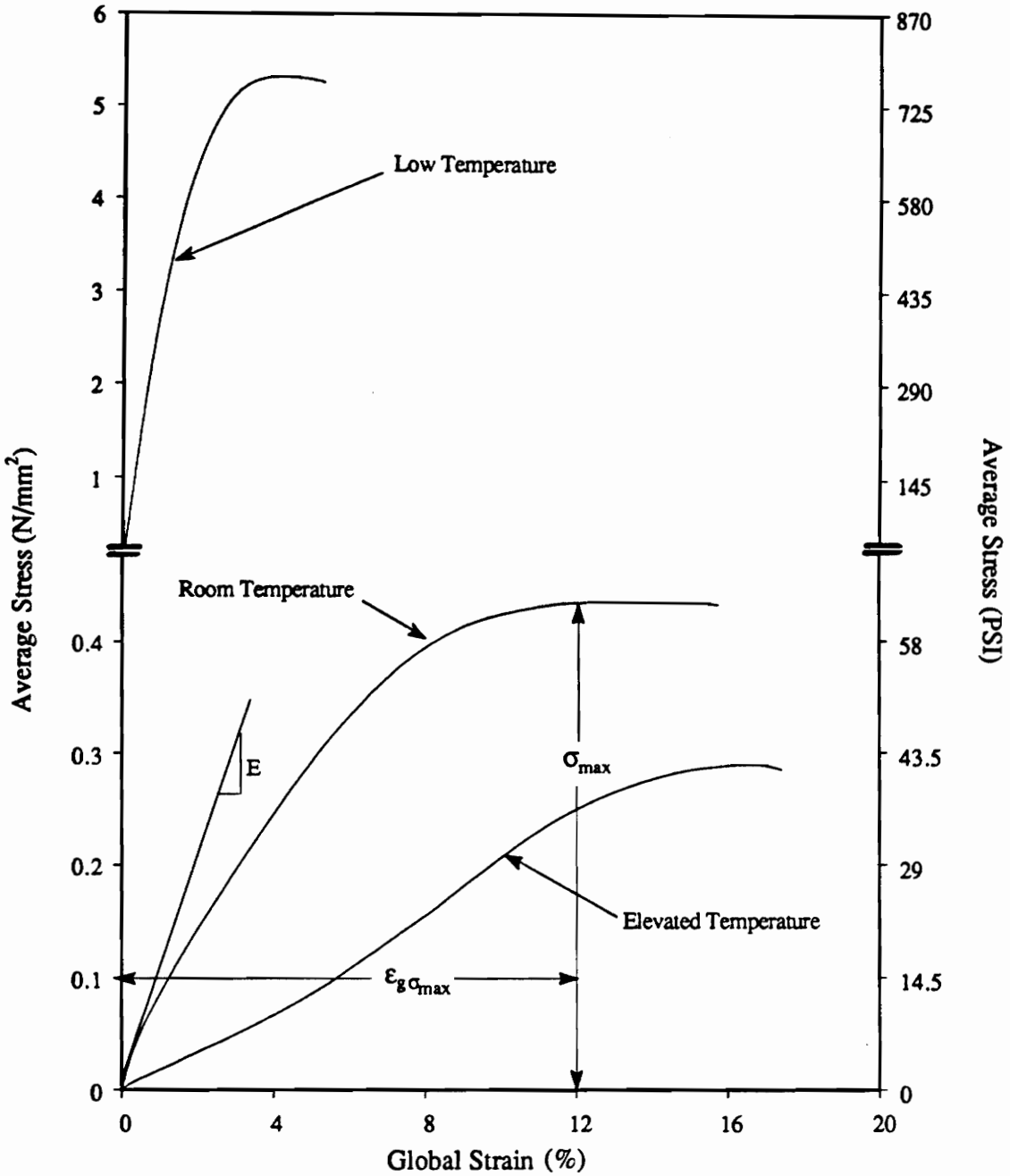

Low, Room and Elevated Temperatures: -65°F, 72°F and 165°F

Figure 4.4. Stress-Strain Curves at -65°F, 72°F and 165°F.

strain curve of a typical solid composite propellant could be divided into two parts. One part was associated with the stretching of the undamaged material and the other part was associated with the stretching of the damaged material. The change from one part to the other corresponded to a significant change in the slope of the stress-strain curve. The strain value corresponding to this change was the dewetting strain ε_d, above which significant dewetting was assumed to occur. In the present case, the dewetting strain ε_d is difficult to determine because the curves are very smooth all the way to fracture. As a result, the curves cannot be easily divided into two parts, as it was done in reference [1]. One may even assume that dewetting takes place in the material as soon as the loading starts. In the present case, an accurate determination of the dewetting strain (and corresponding stress) would require the use of dilatometric methods based on the determination of the volume change associated with dewetting [5,32,33].

The experimental data one can get from the curves consist of the initial Young's modulus, the maximum stress and the strain at maximum stress. These data are summarized in Table 4.2.

It is noticed that temperature has a strong effect upon the mechanical behavior of the material. As temperature increases the material becomes weaker and more compliant; its initial Young's modulus and strength decrease while its elongation at maximum stress increases. However, while the global response of the material is significantly different at -65°F from that at 72°F and 165°F, results from the tests conducted at 72°F and 165°F are much less dissimilar.

Theoretically, the stress-strain curves, the initial Young's modulus, the maximum stress and the strain at maximum stress can be superimposed to yield master curves, using the time-temperature superposition principle. The shift factors to be used are the same as those used for the relaxation modulus curves. In the present case only one head rate and three

Table 4.2. Experimental Data from the Biaxial Tensile Tests Conducted on Uncracked Specimens.

Temperature (°F)	Initial Young's Modulus E (N/mm^2)	Maximum Stress σ_{max} (N/mm^2)	Strain at Maximum Stress $\varepsilon_{g\sigma max}$ (%)
-65	300	5.31	4.5
72	9.44	0.44	11.6
165	1.9	0.29	17.4

temperatures have been considered. As a result, one does not have enough data to plot any meaningful master curve.

4.2 Fracture Behavior

4.2.1 Assessment of the Crack Propagation Process

4.2.1.1 Crack Tip Model

As mentioned in Part 2.3.2.1, a failure process zone generally exists behind the crack tip. An accurate description of the crack propagation process requires the introduction of an apparent and an actual crack tip. As shown in Figure 4.5, the actual crack tip is located just ahead of the failure process zone while the apparent crack tip is located just behind it. Using such a model implies that the actual crack tip is always sharp while the apparent crack tip is necessarily blunted as soon as the failure process zone exists. As explained in the next section, the failure process zone and the actual crack tip cannot always be observed at the free surface. As a result, the crack tip at the free surface, i.e., the point behind which separation of the material is actually observed at the free surface, can either be the actual or the apparent crack tip.

4.2.1.2 Qualitative Description of the Crack Propagation Process

Figures 4.6 and 4.7 show the sequences of the crack propagation process. When it can be observed at the surface of the specimen, the failure process zone appears in the form of a

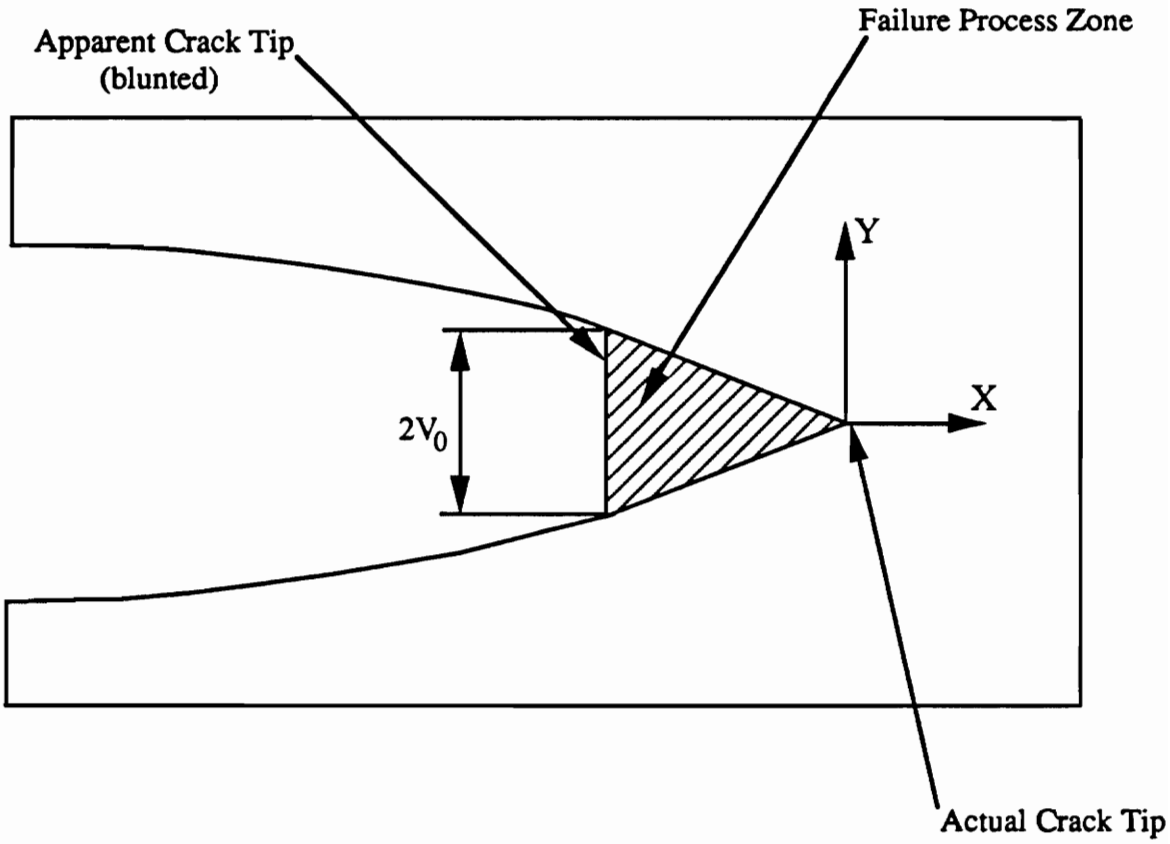

Figure 4.5. Crack Tip Model.

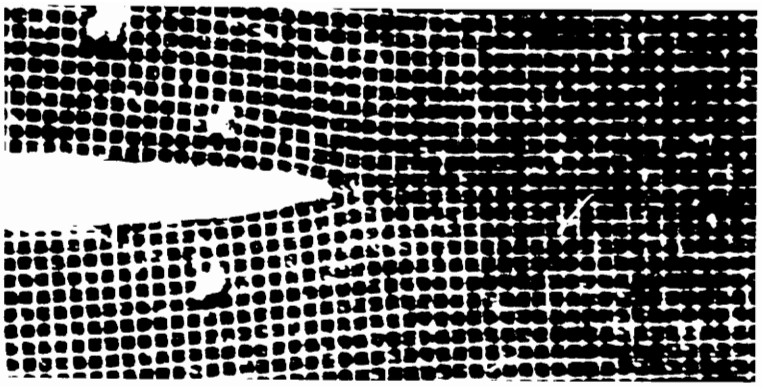

(a) Crack Opening. Global Strain: 0.3%.

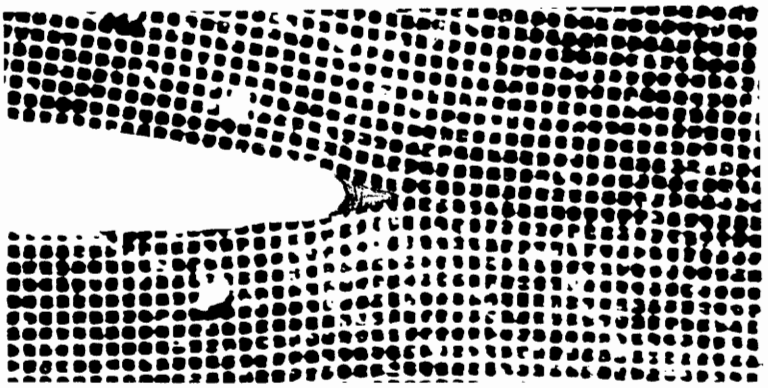

(b) Prior to the Onset of Crack Growth. Global Strain: 1.1%.

(c) Crack Extension. Global Strain: 3.2%.

Figure 4.6. Crack Propagation Process at Low Temperature and High Head Rate.

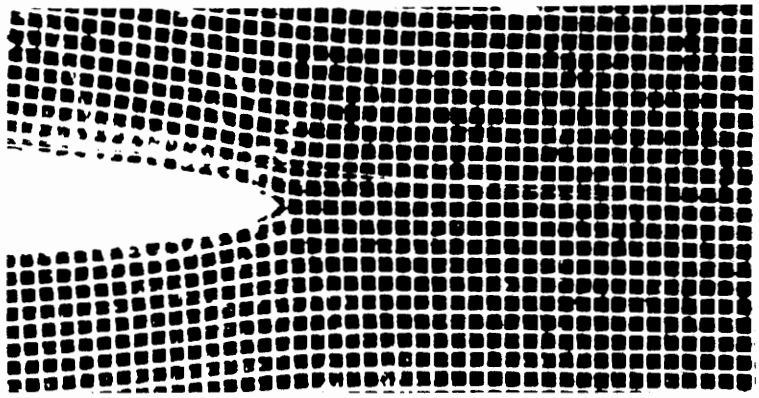

(a) Crack Opening. Global Strain: 5%.

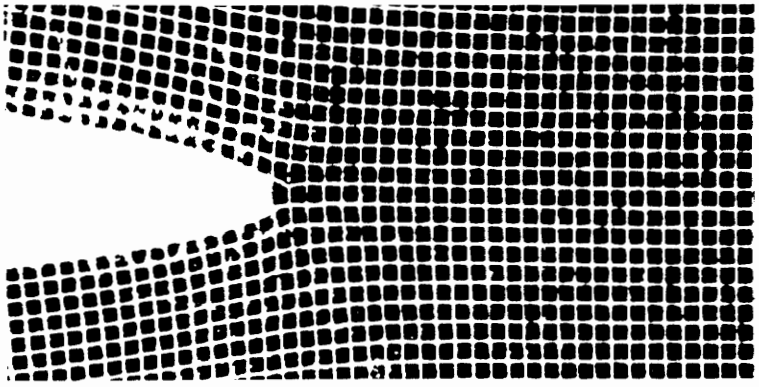

(b) Prior to the Onset of Crack Growth. Global Strain: 7.5%.

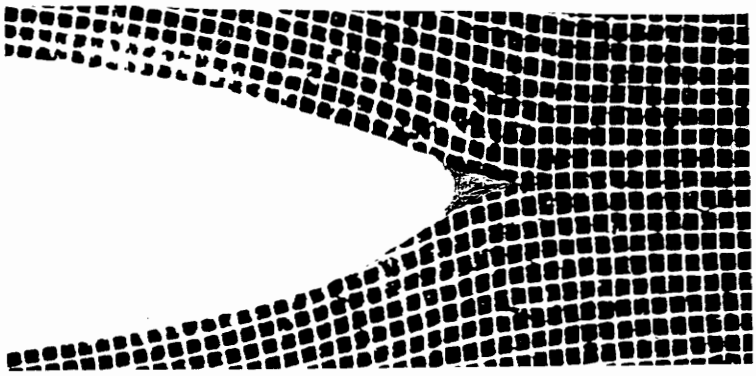

(c) Crack Extension. Global Strain: 11%.

Figure 4.7. Crack Propagation Process at Elevated Temperature and Low Head Rate.

small area in which the grid is significantly damaged. Pictures shown in Figures 4.6 and 4.7 correspond respectively to tests conducted at -65°F with a head rate of 12.7 mm/min. and at 165°F with a head rate of 2.54 mm/min. The crack propagation process was observed to be qualitatively temperature and head rate independent and it can be divided into two stages.

The first stage consists of crack opening and development of the failure process zone ahead of the apparent crack tip. At the beginning of the first stage, the actual and apparent crack tips coincide (Figure 4.7 (a)). As the load increases, the apparent crack tip blunts (Figure 4.6 (a)) and a failure process zone develops just ahead of it. Even though it exists, the failure process zone cannot always be observed at the surface of the specimen (Figures 4.6 (a) and 4.7 (b)). In such cases, the failure process zone is assumed to develop inside the specimen and to be of a very small size. By the end of this first stage, the apparent crack tip is significantly blunted and essentially no crack growth takes place (Figures 4.6 (b) and 4.7 (b)). The failure process zone developing ahead of the apparent crack tip is very localized and probably does not affect the global behavior of the specimen.

The second stage consists of crack growth. At low temperature, the crack growth is relatively fast. The failure process zone and blunting of the apparent crack tip are rarely observed (Figure 4.6 (c)). At room and elevated temperatures the crack growth is much slower. Blunting of the apparent crack tip as well as the failure process zone are seen much more often and are larger than at low temperature (Figure 4.7 (c)). Moreover, at room and elevated temperatures crack propagation is associated with more crack opening than at -65°F. During this second stage, blunting of the apparent crack tip, voiding in the vicinity of the crack tip and presence of the failure zone seem to occur at random at all three temperatures. Generally speaking, the crack grows at an increasing rate and its path is undulated. However, irregularities in the increase of the crack length occur from time to time. These irregularities generally correspond to the presence of voids near the crack tip,

an increase in the blunting of the apparent crack tip or an enlargement of the failure process zone.

Although precise measurements were not made, no evidence of thumbnailing of the crack front could be observed.

4.2.1.3 Quantitative Description of the Crack Propagation Process

Figure 4.8 shows the curves of crack length versus global extension. The effect of temperature on the crack propagation is observed to be much stronger than that of head rate. At low temperature, the crack propagates sooner and faster. The effect of temperature between room and elevated temperatures seems to be small. The effect of head rate on crack propagation seems to be small, except at low temperature where an increase in head rate results in a faster propagation. Based on the rate of crack propagation, the curves of crack length versus global extension can be divided into three parts. The first, second and third parts correspond to no or negligible crack propagation, slow and relatively fast crack propagation, respectively. The limit between the second and third part is based on a qualitative observation of the curves. The first part of the curves corresponds to the first stage of the crack propagation process described above. The two other parts are associated with the second stage.

Figure 4.9 shows the curves of load versus global extension. As in Figure 4.8, the effects of head rate and temperature in the ranges 2.54 mm/min. to 12.7 mm/min. and 72°F to 165°F, respectively, are observed to be quite small, even though they are readily measurable. The curves corresponding to elevated temperature can essentially be described

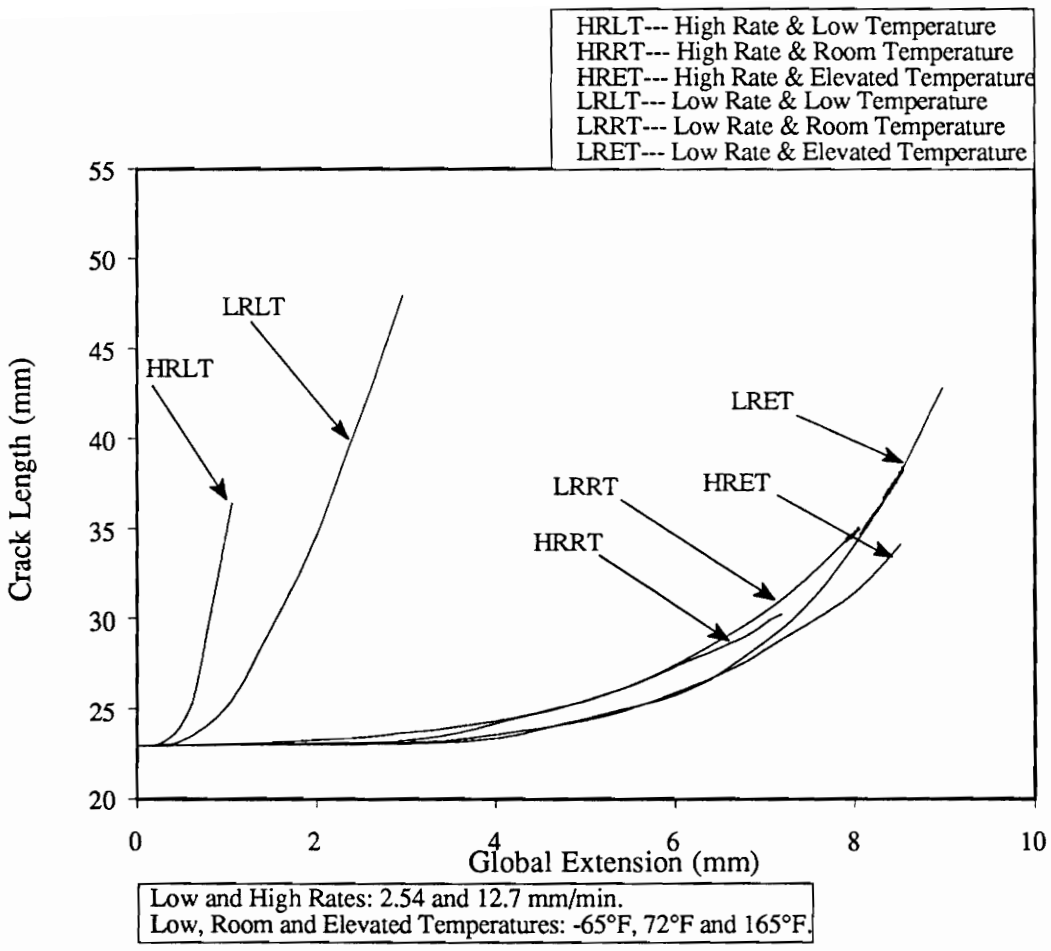

Figure 4.8. Crack Length versus Global Extension.

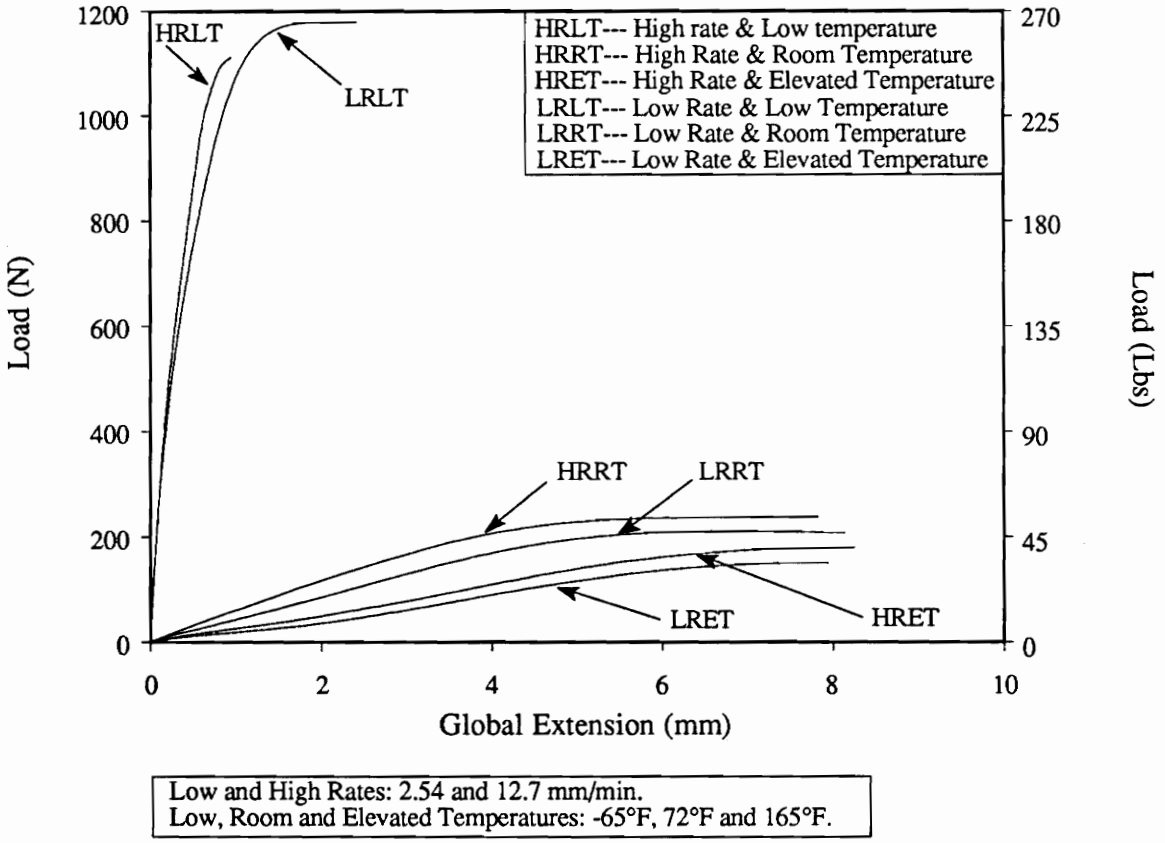

Figure 4.9. Load versus Global Extension.

in the same way as those obtained at low and room temperatures, in spite of their sigmoid shape at small extensions. Based on the rate at which the load increases, the curves of load versus global extension can be divided into three parts. More specifically, the rate at which the load increases is roughly constant in the first part, decreases rapidly during the second part and finally becomes zero by the beginning of the third part. In the third part, the load remains constant for a while and finally drops. The limit between the first two parts is based on a qualitative observation of the curves.

The three parts of the curves showing crack length versus global extension and load versus global extension are observed to correspond to each other. In other words, the first part of the curves load versus global extension is associated with no or negligible crack growth, while the other two parts correspond to propagation of the crack. As a result, the second stage of the crack propagation process described above can be divided into two sequences. The first sequence is a stable and slow crack propagation taking place under an increasing load. The second sequence is a faster and unstable growth, i.e., further crack propagation does not require any increase in load.

Figure 4.10 shows how the loads corresponding to the beginning of stable and unstable crack propagation vary with temperature. Since the effect of the head rate has been found to be small so far, the results corresponding to different head rates at the same temperature have been averaged. One observes that as temperature increases, stable and unstable propagations require lower loads, associated with higher global strains.

In the present case, one notices only a small change in the fracture behavior of the material as temperature drops from 165°F to room temperature, while a significant embrittlement is observed as temperature decreases from room temperature to -65°F. This effect of temperature upon the fracture behavior of the material is consistent with that observed upon

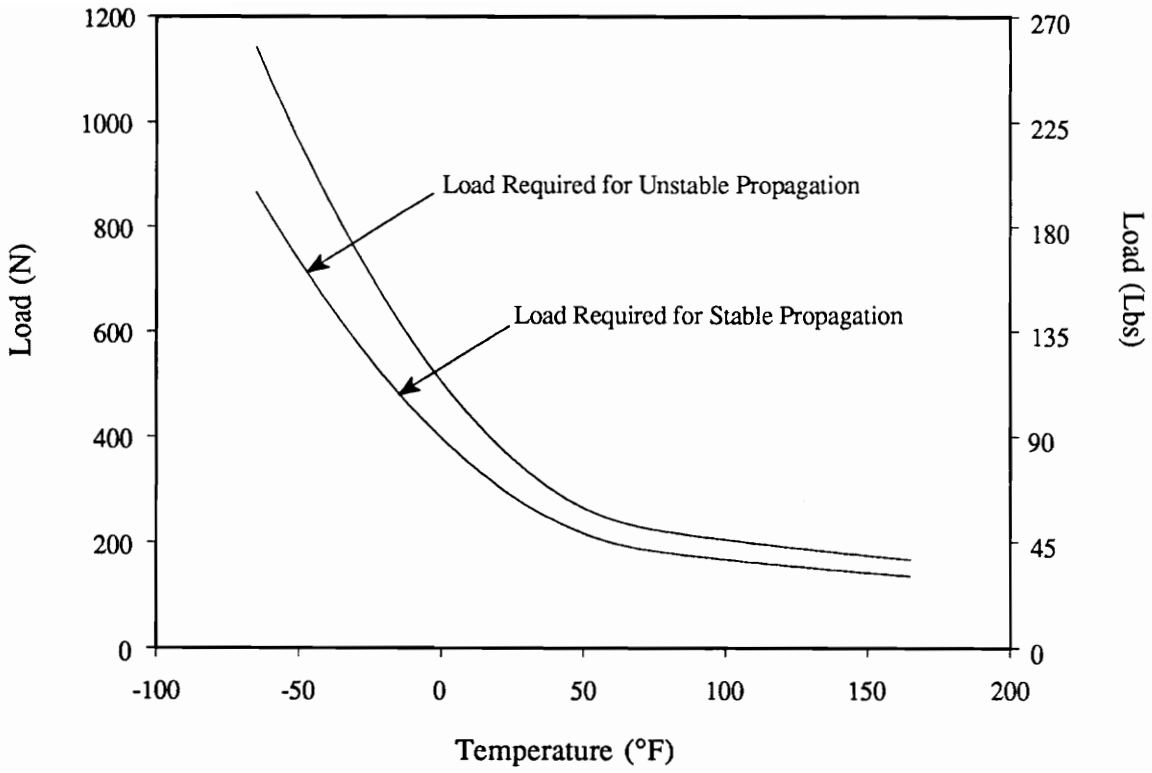

Figure 4.10. Load Required for Stable and Unstable Propagation versus Temperature.

the relaxation behavior and the tensile properties. In the ranges considered, the effect of head rate on crack propagation is much weaker than that of temperature.

4.2.2 Deformation of the Near Tip Region

Typical contour maps of the vertical displacement V and the strains ε_{yy} and ε_{xy} in the near tip region are shown in Figure 4.11. The contours were observed to be qualitatively temperature and head rate independent. As the applied global strain increases, an intense strain zone, i.e., ε_y>15%, develops in the immediate vicinity of the crack tip. This intense strain zone increases in size as the applied global strain increases. In the strain contours, the sharp corners probably result from the error introduced by the method. However, the general shape of the contours, as well as the quantitative information shown in Figure 4.11, are believed to give a reasonable description of the vertical displacement and the strains, ε_{yy} and ε_{xy}, in the near tip region. The complicated shape of the strain contours is believed to result mainly from the heterogeneity of the material due to the presence of the filler particles.

The dominant displacement eigenvalue λ_u at the crack tip was determined for various global strain levels. For sharp crack tips, λ_u was determined using the algorithm described in part 3.5.3.3, while for blunted crack tips the algorithm was modified as follows [35]:

$$V=V_0+Ar^{\lambda_u} \qquad (4.3)$$

whence:

$$\ln(V-V_0)= \ln(A)+\lambda_u\ln(r) \qquad (4.4)$$

where V_0 is half of the blunting (see Figure 4.5).

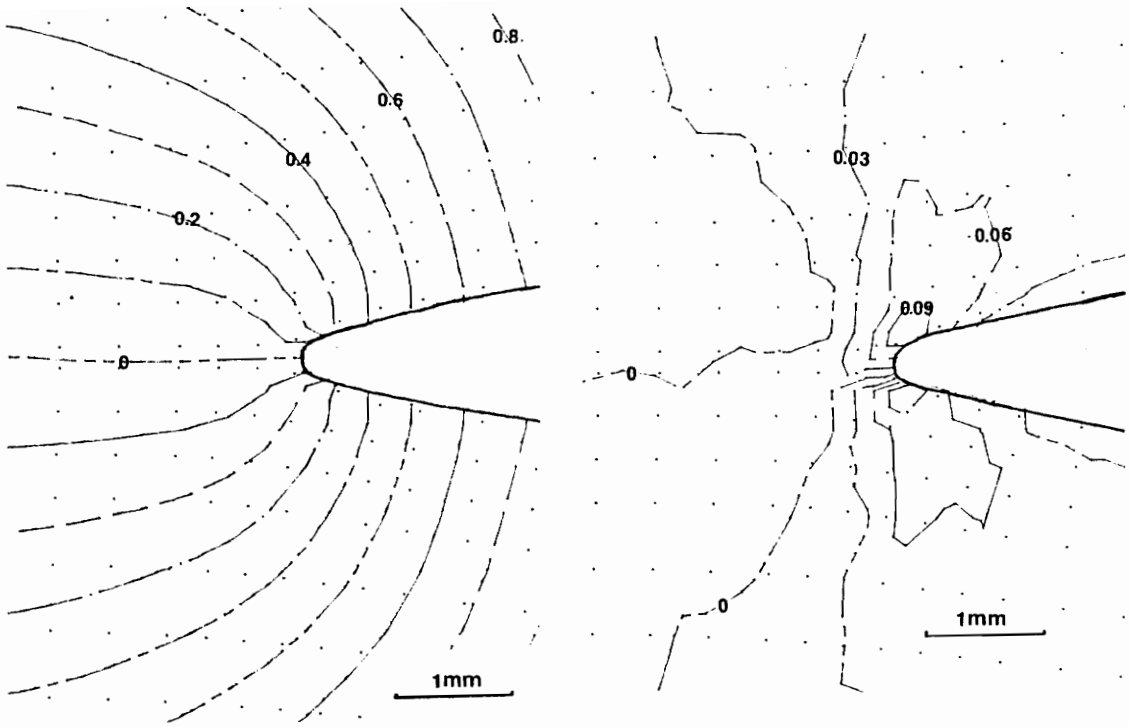

(a) V Displacement Field (mm).

(b) ε_{xy} Strain Field.

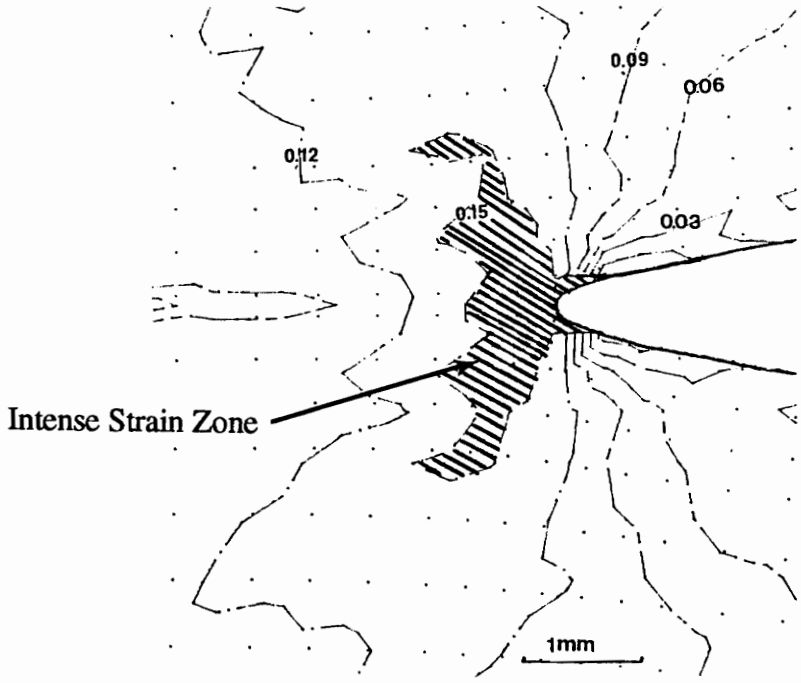

(c) ε_{yy} Strain Field.

Figure 4.11. Near-Tip Displacement and Strain Contours.

The results corresponding to sharp and blunted crack tips are summarized in Tables 4.3 and 4.4, respectively. Figures 4.12 and 4.13 show two typical ln(V) vs ln(r) curves, for sharp crack tips, from which the dominant displacement eigenvalue λ_u can be determined. Figure 4.12 corresponds to a small global strain before crack propagation, while Figure 4.13 corresponds to a higher global strain during crack propagation. As the global strain increases, the inner limit of the linear zone generally moves away from the crack tip. This is consistent with the fact that as the global strain increases, an increasing intense strain zone develops in the vicinity of the crack tip. The values of the dominant displacement eigenvalue λ_u listed in Table 4.3 are in a good agreement with the value of 0.67 predicted by Benthem for incompressible materials. The dominant displacement eigenvalues determined for blunted crack tips are generally higher than that for sharp crack tips. This is consistent with the fact that the stress singularity order at a crack tip theoretically decreases (i.e., the dominant displacement eigenvalue increases) as blunting increases. Accordingly, the value of λ_u should increase as V_0 increases. This trend is not readily verified by the results presented in Table 4.4, probably because the amount of blunting at the crack tip is generally difficult to determine accurately. The lack of accuracy in the determination of V_0 is all the more critical because the modified algorithm (equations 4.3 and 4.4) is very sensitive to the value of V_0.

Generally speaking, reasonable values of λ_u, i.e., values close to 0.67, are obtained provided that the crack tip is sharp and the crack tip as well as the crack plane can be accurately located. This good agreement suggests that the continuum description of the singularity at the crack tip is valid both prior to and during propagation of the crack. The fact that λ_u is observed to be temperature and head rate independent while strongly crack tip geometry dependent proves its singular character.

Table 4.3. Dominant Displacement Eigenvalue λ_u for Sharp Crack Tips.

Temperature (°F)	Head Rate (mm/min.)	Stage of Crack Propagation	λ_u	Linear Zone (mm)
-65	12.7	Crack opening	0.67	0.5- 6.6
-65	12.7	Crack extension	0.73	0.8- 6.8
-65	2.54	Crack opening	0.70	0.1- 6.5
-65	2.54	Crack extension	0.64	0.2- 7.0
72	12.7	Crack opening	0.69	0.3- 6.5
72	12.7	Crack extension	0.63	1.2- 6.5
72	2.54	Crack opening	0.71	0.2- 6.4
72	2.54	Crack extension	0.70	1.4- 7.1
165	12.7	Crack opening	0.76	0.7- 6.4
165	12.7	Crack extension	0.71	1.2- 7.5
165	2.54	Crack opening	0.71	0.4- 6.4
165	2.54	Crack extension	0.70	0.6- 7.2

Table 4.4. Dominant Displacement Eigenvalue λ_u for Blunted Crack Tips.

Temperature (°F)	Head Rate (mm/min.)	Stage of Crack Propagation	λ_u	Linear Zone (mm)	V_0 (mm)
-65	12.7	Crack opening	0.78	0.7- 6.5	0.07
-65	12.7	Crack extension	0.85	0.6- 6.8	0.16
-65	2.54	Crack opening	0.84	1.0- 6.7	0.15
-65	2.54	Crack extension	0.92	1.4- 7.1	0.16
72	12.7	Crack opening	0.85	1.5- 6.6	0.13
72	12.7	Crack extension	-----	----------	------
72	2.54	Crack opening	0.92	1.7- 6.6	0.13
72	2.54	Crack extension	-----	----------	------
165	12.7	Crack opening	0.84	1.4- 6.9	0.14
165	12.7	Crack extension	------	----------	------
165	2.54	Crack opening	0.84	1.8- 6.8	0.10
165	2.54	Crack extension	------	----------	------

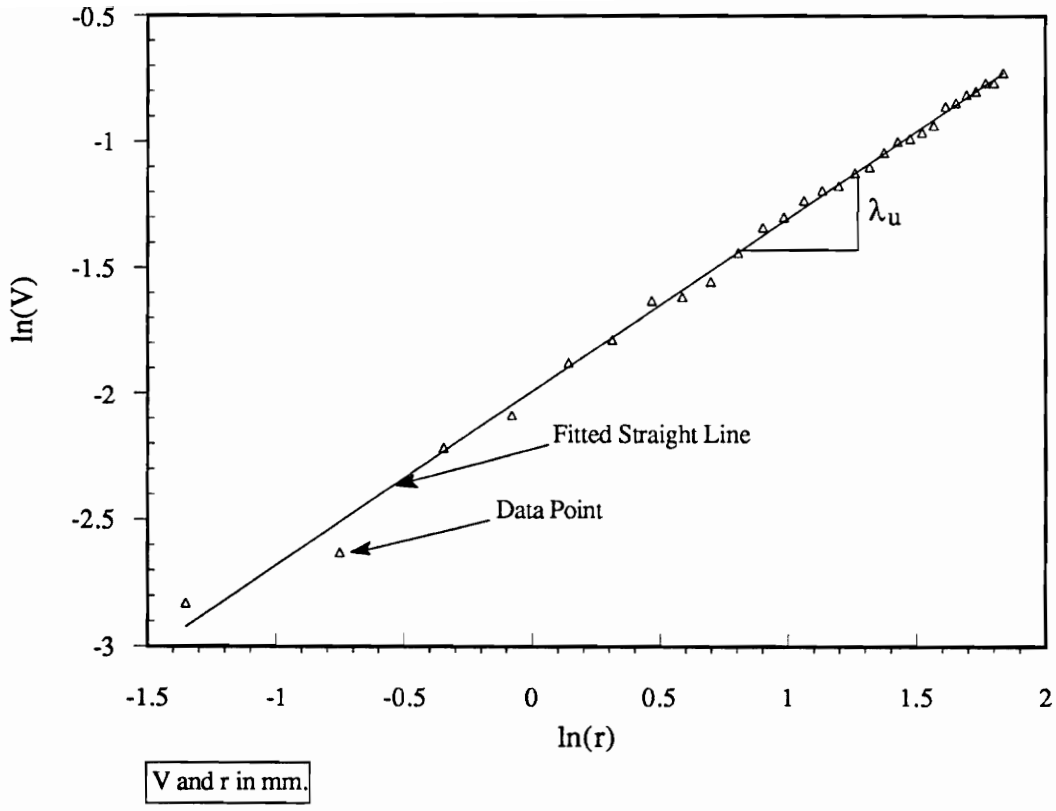

Figure 4.12. Determination of the Dominant Displacement Eigenvalue at Small Global Strain.

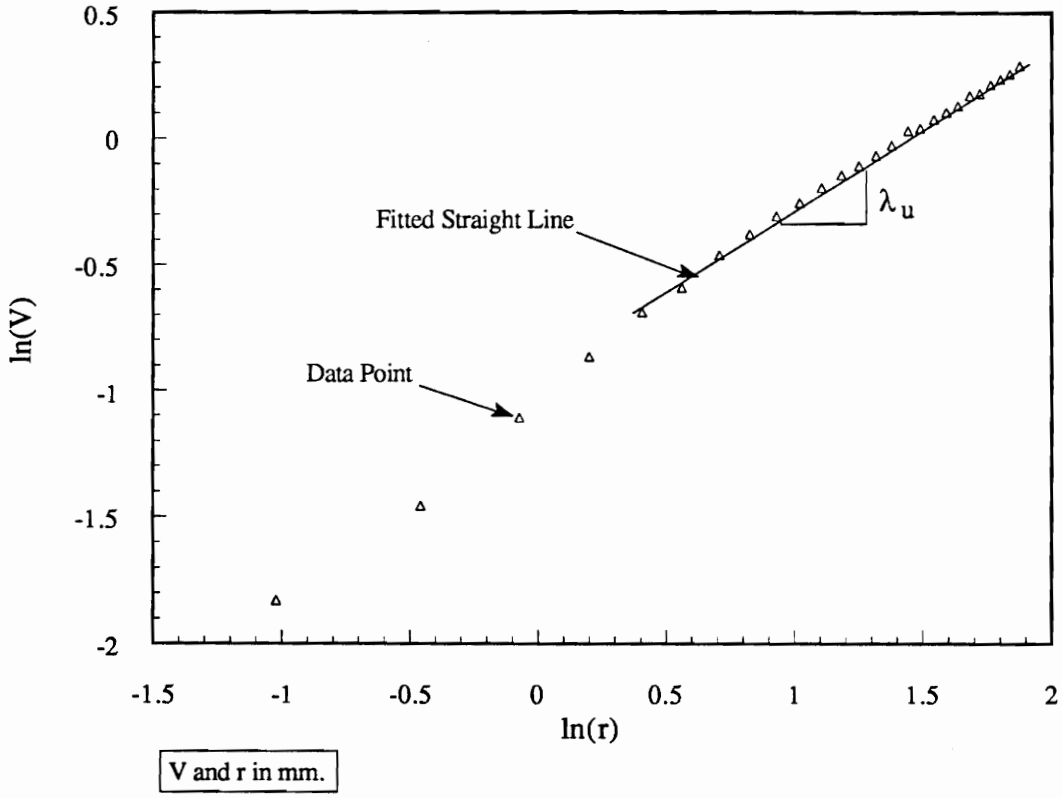

Figure 4.13. Determination of the Dominant Displacement Eigenvalue at Large Global Strain.

4.3 Discussion

4.3.1 Temperature

The temperature limits -65°F and 165°F are the minimum and maximum temperatures to which a rocket motor grain can be exposed during storage and handling prior to operation. Tests were conducted at these two temperatures in order to assess the maximum behavior changes the material could undergo prior to operation.

The mechanical and fracture behavior of the simulated composite solid propellant was observed to vary significantly from -65°F to 165°F. More specifically, an increase in strength and a decrease in extensibility were associated with a decrease in temperature. In addition to a change in the global behavior of the material, the increase of temperature from -65°F to 165°F may also result in physical changes in the binder. This was suggested by the sigmoid shape of the stress-strain curve at low strains at 165°F (see Figures 4.4). This sigmoid shape is characteristic of soft elastomer and may be due to a process of crystallization taking place in the binder as it is stretched at elevated temperature.

In addition to the tests conducted at -65°F and 165°F, tests were also performed at room temperature (72°F). The global behaviors of the material at 72°F and 165°F were observed to be very similar, even though the stress-strain curve at 72°F did not exhibit the sigmoid shape at low strains. As a result, the mechanical and fracture behavior of the material at 165°F can be reasonably assessed by conducting tests at room temperature. This is of interest when one considers that conducting tests at room temperature is easier than at 165°F. In other words, a study of the mechanical and fracture behavior of composite solid propellant in the temperature range -65°F to 165°F can be approximated by conducting tests at temperatures ranging from -65°F to room temperature (72°F).

4.3.2 Filler Particles and Resistance to Local Dewetting

In reference [34], Rezvani presented data corresponding to crack propagation tests conducted at room temperature, on biaxial specimens of pure binder and simulated solid propellant. Rezvani noticed that blunting of the apparent crack tip was significant in the simulated solid propellant, while negligible in the pure binder. However, as suggested by Schapery [16], blunting of the apparent crack tip is believed to occur in both pure binder and composite solid propellant. Blunting of the apparent crack tip results from the development of a failure process zone ahead of the apparent crack tip. In pure binder, the damage in the failure process zone consists of crazing (or voiding) only, while in composite solid propellant it consists of dewetting and crazing within the binder. Using the crack tip model shown in Figure 4.5, it is reasonable to assume that the amount of blunting of the apparent crack tip is related to the size of the failure process zone: the larger the failure process zone, the more severe the blunting. As a result, the presence of the filler particles seems to promote blunting of the apparent crack tip by enlarging the failure process zone.

In reference [35], the crack propagation process in a simulated composite solid propellant was investigated at room and elevated temperatures. In that case, crack propagation was associated with severe blunting of the apparent crack tip and extensive microcracking in the near tip region. In the present case, blunting of the apparent crack tip is generally not severe and microcracks in the near tip region are rarely observed. As a result, blunting of the apparent crack tip and development of microcracks in the near tip region seem to be closely related. The microcracks developing in the near crack tip region are believed to result mainly from local dewetting. Consequently, the fact that, in the present case, fewer

microcracks are observed in the near tip region indicates that the material has a higher resistance to local dewetting.

The severity of blunting of the apparent crack tip appears to be related to the presence of filler particles and microcracking in the near tip region. More specifically, one can infer that the severity of blunting of the apparent crack tip is related to the resistance of the material to local dewetting. This relationship can be explained as follows: an increased resistance of the material to local dewetting reduces the formation of voids in the failure process zone, resulting in a decrease in the size of the failure process zone and the amount of blunting of the apparent crack tip.

Considering that the dewetting process weakens as temperature decreases [6], the previous conclusion is consistent with the fact that blunting of the apparent crack tip was less severe at -65°F than at room and elevated temperatures.

The filler particles seem to be also responsible for the undulation of the crack propagation path. indeed, since the binder is weaker than the filler particles, the crack propagates only in the binder or at the interface between binder and particles. Consequently, as it propagates, the crack has to pass by the filler particles, resulting in an undulated path.

4.3 Determination of the Dominant Displacement Eigenvalue

The use of the modified algorithm (equations 4.3 and 4.4) for a blunted crack tip generally leads to a dominant displacement eigenvalue higher than that obtained for a sharp crack tip. Even though, from a physical stand point, this observation does make sense, there is no certainty that equations 4.3 and 4.4 allow one to accurately account for the blunting of the crack tip. Since, in the case of a blunted crack tip, no theoretical prediction is available for comparison with the experimental results, the determination of the dominant displacement eigenvalue λ_u in the case of a blunted crack tip is open.

5.0 Closure

5.1 Conclusion

The mechanical and fracture behavior of a simulated composite solid propellant was investigated. Stress relaxation, constant head rate and crack propagation tests were conducted on biaxial tensile specimens. The effects of temperature and head rate were assessed by conducting tests at three temperatures (-65°F, room temperature (72°F) and 165°F) and two head rates (2.54 and 12.7 mm/min.). Major conclusions are listed below:

1) In the range -65°F to 72°F, temperature significantly influences the behavior of the material. As temperature decreases, the material becomes more brittle: it becomes stronger and less extensible and crack propagation through it is faster. In the range 72°F to 165°F, the influence of temperature upon the behavior of the material is small. As a result, the assessment of the mechanical and fracture behavior of the material over the range -65°F to 165°F can be reasonably achieved by conducting tests over the range -65°F to 72°F only.

2) In the range 2.54 mm/min. to 12.7 mm/min., the influence of the head rate on the mechanical and fracture behavior of the material, while readily measurable, is quite small.

3) In the ranges of temperatures and head rates investigated, the crack propagation process is qualitatively temperature and head rate independent. The severity of the blunting of the

apparent crack tip associated with the development of a failure process zone ahead of it both before and during crack extension seems to be related to the resistance of the material to local dewetting. More specifically, an increased resistance to local dewetting is believed to result in less blunting at the apparent crack tip, and vice versa.

4) The use of a continuum algorithm to determine the dominant displacement eigenvalue at the free surface led to reasonable results for sharp crack tips.

5.2 Recommendations and Future Work

A few recommendations and ideas for future work are listed below:

1) As mentioned earlier, the determination of the dominant displacement eigenvalue λ_u at the free surface is open in the case of a blunted crack tip. As a result, it is of interest to further study the effect of blunting on the dominant displacement eigenvalue and to assess how accurately the modified algorithm (equations 4.3 and 4.4) accounts for the blunting of the crack tip.

2) The complicated shape of the strain contours (see Figures 4.11 (b) and (c)) is believed to be due to the error introduced by the method and to the presence of the stiff filler particles. Because the separation of the error introduced by the method from the effect of the presence of the filler particles is not straightforward, one has to minimize the error introduced by the method in order to make it negligible. To achieve such a goal, the use of a hybrid method involving the finite element method and experimental results is currently under investigation.

3) The present study results in the assessment of the mechanical and fracture behavior of a typical composite solid propellant as temperature varies from -65°F to 165°F, i.e., from the minimum to the maximum temperature a solid rocket motor grain can be subjected to prior to and shortly after ignition. Using a model of a rocket motor grain, the effects of the

geometry of the grain upon the propagation of surface flaws in the grain are currently investigated in the laboratory. The next step consists of gathering the geometry and material effects upon crack propagation in order to study the behavior of surface flaws in actual rocket motor grains prior to and shortly after ignition.

References

1. Sutton, G.P., "Rocket Propulsion Elements," fifth ed., John Wiley & Sons, 1986, Chap.10 and 11.
2. Britton, S.C., "Characterization of Solid Propellants as Structural Materials," Solid Rocket Structural Integrity Abstracts, Vol. II, No. 4, 1965.
3. Durelli, A.J., "Development of Experimental Stress Analysis Methods to Determine Stresses and Strains in Solid Propellant Grains," Interim Report No.6, Office of Naval Research, March 1965.
4. Williams, M.L., "Structural Analysis of Viscoelastic Materials," Solid Rocket Technology, Edited by Shorr, 1967.
5. Kruse, R.B., "Laboratory Characterization of Solid Propellant Mechanical Properties," AIAA 65-147, 1965.
6. Bills, K.W., and Wiegand, J.H., "Relation of Mechanical Properties to Solid Rocket Motor Failure," AIAA Journal, Vol. 1, No. 9, 1963, pp. 2116-2123.
7. Jones, T.M. and Kruse, R.B.,"Failure Behavior of Composite Hydrocarbon Fuel Binder Propellants," AIAA 65-156, 1965.
8. Aklonis, J.J., "Introduction to Polymer Viscoelasticity," Second Edition, John Wiley and Sons, 1983.
9. Plazek, D.J., "Temperature Dependence of the Viscoelastic Behavior of Polystyrene," The Journal of Physical Chemistry, Vol. 69, No. 10, 1965, pp. 3480-3487.
10. Sperling, L.H., "Introduction to Physical Polymer Science," John Wiley & Sons, 1986.

11. Williams, M.L., Landel, R.F. and Ferry, J.D., "The Temperature Dependence of Relaxation Mechanisms in Amorphous Polymers and Other Glass-forming Liquids," Journal of the American Chemical Society, 77, 1955, pp. 3701-3707.

12. Ferry, J.D., "Viscoelastic Properties of Polymers," Third ed., John Wiley & Sons, 1980.

13. Liu, C.T., "Non-Destructive Evaluation of Near Tip Damage Fields in a Composite Solid Propellant," International Conference on Computational Engineering Science, 1988.

14. Liu, C.T., "Investigating the Local Behavior Near the Crack Tip in a Composite Solid Propellant," Society of Experimental Mechanics, Spring Conference, 1989, pp. 491-496.

15. Liu, C.T., and Yang, J.N. "A Probabilistic Crack Growth Model for Application to Composite Solid Propellants," AIAA 91-0917, 1991.

16. Schapery, R.A., "A Theory of Crack Initiation and Growth in Viscoelastic Media. Part I," International Journal of Fracture, 11, 1975, pp. 141-159.

17. Schapery, R.A., "A Theory of Crack Initiation and Growth in Viscoelastic Media. Part II," International Journal of Fracture, 11, 1975, pp. 369-388.

18. Schapery, R.A., "A Theory of Crack Initiation and Growth in Viscoelastic Media. Part III," International Journal of Fracture, 11, 1975, pp. 549-562.

19. Liu, C.T., "Crack Growth Behavior in a Composite Propellant with Strain gradients. Part I," AIAA 84-1294, 1984.

20. Liu, C.T., "Crack Growth Behavior in a Composite Propellant with Strain Gradients. Part II," AIAA 85-0615, 1985.

21. Liu, C.T., "Crack Propagation in a Composite Solid Propellant," Society of Experimental Mechanics, Spring Conference, 1990, pp. 614-620.

22. Swanson, S.R., "Application of Schapery's Theory of Viscoelastic Fracture to Solid Propellant," Journal of Spacecraft and Rockets, Vol. 13, No. 9, 1976, pp. 528-533.

23. Schapery, R.A., "Fracture Mechanics of Solid Propellants," Fracture Mechanics-10th Symposium on Naval Structural Mechanics, 1978, pp 387-398.

24. Benthem, J.P., "Three Dimensional State of Stress at the Vertex of a Quarter-Infinite Crack in a Half-Space," Report WTHD No. 74, Delft Univ. of Tech., The Netherlands, 1975.

25. Benthem, J.P., " State of Stress at the Vertex of a Quarter-Infinite Crack in a Half-Space," International Journal of Solids and Structures, Vol. 13, 1977, pp. 479-492.

26. Benthem, J.P., "The Quarter Infinite Crack in a Half Space; Alternative and Additional Solutions," International Journal of Solids and Structures, Vol. 16, 1980, pp. 119-130.

27. Obata, M., Shimada, H., and Kawasaki, A., "Fine-Grid Method for Large-Strain Analysis Near a Notch Tip," Experimental Mechanics, Vol. 23, No. 2, 1983, pp. 146-151.

28. Smith, C.W., Rezvani, M., and Liu, C.T., "Measurement of Fracture Parameters in Polyphase Materials," Micromechanics: Experimental Techniques, ASME, Vol. 102, 1989, pp. 107-119.

29. Czarnek, R., Post, D., and Lee, J.,"Experimental Analysis of the Failure Process of Simulated Solid Rocket Propellant," Society of Experimental Mechanics, Spring Conference, 1988, pp. 454-458.

30. Post, D., Smith, C.W., and Czarnek, R., "Crack Opening and Extension in Inert Solid Propellant: an Experimental Study," Report AFAL-TR-87-043, 1987.

31. Post, D., Smith, C.W., and Czarnek, R., "Boundary Layer and Singularity Measurement in Three Dimensional Fracture Problems," Report AFAL-TR-88-086, 1988.

32. Wiegand, J.H., "Recent Advances in Mechanical Properties Evaluation of Solid Propellants," ARS Journal, April 1962, pp. 521-527.

33. Farris, R.J., "Dilatation of Granular Filled Elastomers under High Rates of Strain," Jounal of Applied Polymer Science, Vol. 8, pp. 25-35, 1964.

34. Rezvani, M.A., "A Study of Near Tip Phenomena for Cracks in a Particulate Composite," PhD Dissertation, VPI & SU, April 1989.

35. Smith, C.W., Wang, L. and Mouille, H., "Observation of Material and Geometric Effects on Crack Opening and Growth for Particulate Composite," Symposium on Experiments in Micromechanics of Failure, ASME-WAM, Atlanta, December 1991.

Vita

The author was born on June 10, 1967 in Cluses, France. He graduated from Cluses High School in June 1985 and received his bachelor's degree from Ecole Nationale Supérieure d'Arts et Métiers (Paris, France) in June 1990. The author came to Virginia Tech, prior to graduate from college, in July 1989. In August 1990, the author started his graduate education in Engineering Science and Mechanics at Virginia Tech.

Since then, the author has been working with prof. C.W. Smith, studying Fracture Mechanics by experimental techniques.

Hervé Mouille